The Biological Pump and Seasonal Variability of pCO2 in the Southern Ocean: Exploring the Role of Diatom Adaptation to Low Iron

Renaud Person, Olivier Aumont, Marina Lévy

The Biological Pump and Seasonal Variability of pCO_2 in the Southern Ocean: Exploring the Role of Diatom Adaptation to Low Iron

R. Person[1], **O. Aumont**[1], **and M. Lévy**[1]

[1]Sorbonne Universités, UPMC Université Paris 06, CNRS, IRD, MNHN, UMR 7159 LOCEAN-IPSL, Paris, France

Key Points:
- First sensitivity study of the physiological adaptation of Southern Ocean diatoms to low iron in a biogeochemical model
- The adaptive strategy of diatoms increases primary production and strengthens the biological pump in the Southern Ocean
- This physiological adaptation has significant impacts on the simulated seasonal cycles of chlorophyll and pCO_2 in the Southern Ocean

Correspondence to:
R. Person,
renaud.person@locean-ipsl.upmc.fr

Abstract Iron is known to limit primary production in the Southern Ocean (SO). To cope with the lack of this micronutrient, diatoms, a dominant phytoplankton group in this oceanic region, have been shown in cultures to have developed an original adaptation strategy to maintain efficient growth rates despite very low cellular iron quotas, even in low light conditions. Using a global ocean biogeochemical model, we explored the consequences of this physiological adaptation for the biological pump and the seasonal variability of both surface chlorophyll concentrations and surface partial pressure of carbon dioxide (pCO_2) in this key region for global climate. In the model, we implemented a low intracellular Fe:C requirement in the SO for diatoms uniquely. This results in an increase of 10% in the relative contribution of diatoms to total SO primary production. The biological pump is also strengthened, which increases the biological contribution to the seasonal evolution of pCO_2 relative to the thermodynamic component. Therefore, the seasonal evolution of both surface chlorophyll and surface pCO_2 is significantly impacted, with a marked improvement, in our model, in the SO polar zone compared to the observations. Our model study underscores the potentially important consequences that this adaptive physiological behavior of diatoms could have on marine biogeochemistry in the SO. It is thus critical to improve our understanding of the physiology of this key phytoplankton group, in particular in the SO.

1. Introduction

The SO is a key region for the global carbon cycle and the climate system that contributes significantly to the uptake of both anthropogenic (Khatiwala et al., 2013; Sabine et al., 2004) and natural carbon dioxide (CO_2) (Metzl et al., 2006; Takahashi et al., 2009). Nevertheless, large uncertainties remain regarding the drivers and the magnitude of this uptake partly due to the lack of observations at the seasonal scale (Gruber et al., 2009; Lenton et al., 2006, 2013; Metzl et al., 2006), a direct consequence of the remote situation and the stormy nature of this region. Observations indicate that seasonality is the main mode of variability of pCO_2 in the SO (Lenton et al., 2006; Thomalla et al., 2011), which is driven by a combination of biological, physical, and thermodynamic processes that act at different time scales from seasonal to subseasonal and are highly variable in space (Lenton et al., 2006; Monteiro et al., 2015; Resplandy et al., 2014; Shadwick et al., 2015; Takahashi et al., 2012). Modeling and disentangling the balance between these different processes have proved challenging as illustrated by the large spread in the phasing and amplitude of the seasonal cycle of pCO_2 simulated by CMIP5 models in different parts of the SO (Anav et al., 2013; Lenton et al., 2013; Majkut et al., 2014). A recent study provided a methodological framework to elucidate the reasons for such large differences. This methodology, which has been applied to the ocean biogeochemical component of one of these CMIP5 models (NEMO-LIM2-PISCES), shows an underestimation of both the biological pump and the winter entrainment of CO_2, relative to the solubility effect in the SO (Mongwe et al., 2016).

Properly resolving the seasonal variability of pCO_2 in the SO is a prerequisite for reliable assessments of the global carbon budget and for relevant climate projections (Landschützer et al., 2014; Lenton et al., 2012; Majkut et al., 2014; Metzl et al., 2006; Takahashi et al., 2009). Therefore, it is crucial to identify the key processes that contribute significantly to the variability of air-sea CO_2 exchanges. Due to its complexity and the many poorly known processes that drive its variability, a proper integration and representation of the biological component in ocean biogeochemical models is one of the great challenges for the prediction of the response of the marine ecosystems and of the biogeochemical cycles to climate change.

A key feature of the SO is that it is the largest High Nutrient Low Chlorophyll (HNLC) region, i.e., where a large availability in macronutrients is associated with a relatively weak phytoplankton biomass (Comiso et al., 1993; Moore & Abbott, 2000), especially in the open ocean south of 50°S (Tagliabue et al., 2012). As hypothesized by Martin et al. (1990), and confirmed by *in situ* mesoscale iron fertilization experiments (Boyd et al., 2007), low availability of iron limits the growth of phytoplankton at large scale in the SO. However, despite the overall general HNLC conditions that prevail in the SO, intense algal blooms can be observed in spring and summer (Sullivan et al., 1993), for instance, in the vicinity of the Crozet archipelago (Pollard et al., 2009) and of South Georgia Island (Borrione & Schlitzer, 2013; Korb et al., 2008), over the Kerguelen Plateau (Blain et al., 2008), in coastal polynyas and during the summer retreat of sea-ice (Arrigo et al., 1999, 2015; Arrigo & van Dijken, 2003; Smith et al., 2008).

Diatoms, a dominant phytoplankton group in the SO (Armbrust, 2009; Arrigo et al., 1999; Pondaven et al., 2000; Rigual-Hernández et al., 2015b), are recognized to play a key role in the oceanic carbon cycle (Falkowski et al., 1998; Smetacek, 1999). They account for up to 40% of the global primary production in the ocean (Nelson et al., 1995; Smetacek, 1999; Tréguer & Pondaven, 2000), a contribution estimated to as much as 89% in the SO (Rousseaux & Gregg, 2013). Partly due to their silica shell and their large size, diatoms dominate the export of carbon in many areas of the SO (Assmy et al., 2013; Buesseler et al., 2001; Pollard et al., 2009; Rembauville et al., 2015, 2016; Rigual-Hernández et al., 2016; Salter et al., 2012) and hence, affect the efficiency of the biological pump (Tréguer et al., 2017), which is the process by which newly fixed organic carbon is sequestered from the upper layer of the ocean, mainly through settling particles.

Since iron is a key limiting factor for primary production in HNLC regions, its availability shapes the spatial and temporal patterns of the ocean productivity in these regions by altering the physiology of marine phytoplankton (Boyd, 2002; de Baar, 2005). The Fe:C quota of diatoms exhibits a wide range of values (Marchetti et al., 2006; Sarthou et al., 2005), which reflects the environmental conditions as well as the variability in the iron requirements to sustain the growth of this eukaryotic phytoplankton group. Several studies have shown that oceanic diatoms are able to reduce their iron requirements under iron limiting conditions in comparison with coastal species (Kustka et al., 2007; Marchetti et al., 2006; Strzepek & Harrison, 2004). Accordingly, laboratory studies suggest that several diatom species from the SO have developed a specific adaptive strategy (Strzepek et al., 2011, 2012). Indeed, in cultures, the intracellular Fe content and Fe:C ratios of four SO diatoms were found to display exceptionally low values, at least two fold lower than currently reported for oceanic algal species such as *Phaeocystis* (Strzepek et al., 2011). When compared to diatom species from temperate latitudes, SO diatoms were found to require lower cellular iron concentrations and Fe:C ratios to achieve comparable growth rates and their iron requirements decreased or remained relatively constant with decreasing light levels (Strzepek et al., 2012).

For now, this adaptation strategy of SO diatoms is not yet accounted for in any biogeochemical models. In this study, we sought to characterize and quantify the sensitivity of the seasonal variability of the air-sea CO_2 fluxes in the SO to this adaptation strategy. For that purpose, we used a global configuration of a coupled ocean physical and biogeochemical model. We show that accounting for this behavior of SO diatoms has large impacts on the biological pump that lead to significant changes in the simulated seasonal cycles of both surface chlorophyll concentrations and pCO_2. These results have important implications for the evaluation of air-sea CO_2 exchanges in climate models and stress the role played by SO diatoms in the carbon cycle. Our study also highlights the influence of the availability of iron on the physiology and the demand of phytoplankton and the strong impacts this influence has on primary production in biogeochemical models.

2. Method

2.1. Ocean Biogeochemical Model: NEMO-PISCES

We used the hydrodynamical and biogeochemical model NEMO (Nucleus for European Modelling of the Ocean) version 3.6 (Madec, 2008). The model couples the ocean dynamical code OPA (Madec, 2008), the sea-ice model LIM2 (Timmermann et al., 2005), and the marine biogeochemical model PISCES-v2 (Pelagic Interaction Scheme for Carbon and EcosystemStudies) (Aumont et al., 2015). We used NEMO in a global configuration with a nominal horizontal resolution of 2° with increased 0.5° latitudinal resolution at the equator (ORCA2 grid). The vertical grid has 31 levels with 10 levels in the upper 100 m and adopts a partial

step z-coordinate scheme. Lateral mixing along isopycnal surfaces is computed as in Lengaigne et al. (2003). Baroclinic instabilities follow the Gent and McWilliams (1990) parametrization and vertical mixing is parameterized using the turbulent kinetic energy scheme (Gaspar et al., 1990) as modified by Madec (2008).

The dynamical state of the ocean simulated by NEMO drives the PISCES model in an offline mode as described in Aumont et al. (2015). PISCES simulates the lower trophic levels of the marine ecosystem with two phytoplankton compartments (diatoms and nanophytoplankton), two zooplankton size-classes (microzooplankton and mesozooplankton) and the biogeochemical cycles of carbon and of the main nutrients (N, P, Fe, and Si). Phytoplankton growth in PISCES-v2 (Aumont et al., 2015) is parameterized according to a mixed Monod-quota approach: phytoplankton growth rate is limited by the external availability of N and P for both groups, of Si for diatoms, and by the internal availability of iron (Fe quota), which means that the iron quota is variable. The iron limitation term for phytoplankton (nanophytoplankton and diatoms) is modeled according to a classical quota formulation:

$$L_{Fe}^{P}=\min\left(1,\max\left(0,\frac{\theta^{Fe,P}-\theta_{\min}^{Fe,P}}{\theta_{\mathrm{opt}}^{Fe,P}}\right)\right)$$

where $\theta^{Fe,P}$ is the iron quota of phytoplankton (P) modeled as described in Aumont et al. (2015) and $\theta_{\mathrm{opt}}^{Fe,P}$ is the optimum iron quota. This formulation allows for luxury uptake of iron following the modeling framework proposed by Buitenhuis and Geider (2010). In this equation, the minimum iron quota, $\theta_{\min}^{Fe,P}$, denotes the minimum iron requirement of phytoplankton to achieve photosynthesis, respiration, and nitrate/nitrite reduction. In the standard version of the model, $\theta_{\min}^{Fe,P}$ follows the parametrization proposed by Flynn and Hipkin (1999) as adapted by Aumont et al. (2015) which predicts values typically between 7 and 15 μmol Fe mol C^{-1} for diatoms in the SO. These values of the minimum iron quota are significantly larger, by up to a factor of 10, than what has been evidenced in cultures by Strzepek et al. (2011, 2012).

In order to account for the specific adaptation of diatoms to the low availability of iron in the SO, we modified the $\theta_{\min}^{Fe,P}$ formulation south of 30°S. More specifically, we fixed $\theta_{\min}^{Fe,P}$ at a constant value of 2 μmol Fe mol C^{-1} south of 45°S. This corresponds to the upper range of the smallest ratios that have been estimated for four SO diatom species in the culture studies of Strzepek et al. (2011, 2012). The choice of a constant value reflects the observed relative independence of the minimum iron requirements of diatoms to light levels (Strzepek et al., 2012). A transition zone was defined between 30°S and 45°S where a linear interpolation was applied between $\theta_{\min}^{Fe,P}$ computed according to Flynn and Hipkin (1999) and the constant minimum value imposed south of 45°S.

The model was initialized with World Ocean Atlas 2009 annual climatologies for nutrients (nitrate, phosphate, and silicate) and oxygen, GLODAP-v1 annual climatologies for DIC and alkalinity and with preindustrial atmospheric CO_2 concentration (280 ppm). Two model experiments have been performed: one with the standard version of the model (CTL) and one with the modifications described above (PHYSIO). Each model configuration has been integrated for more than 3,000 years to achieve a quasi-balanced state for the air-sea CO_2 fluxes. Following these spin-up runs, both experiments have been forced by historical atmospheric CO_2 concentrations where atmospheric CO_2 is increased from 287.3 ppm (year 1860) to 378.6 ppm (year 2010).

The relative contribution of the thermodynamical, biological, and physical processes to the seasonal cycle of pCO_2 was decomposed into two main drivers of this variability: the solubility effect on one hand and the biological and physical factors on the other hand. The relative contribution of temperature (solubility effect) was computed following the formulation of Takahashi et al. (1993):

$$\frac{(\partial pCO_2/\partial T)}{pCO_2}=0.0423^{\circ}C^{-1}$$

The biological and physical relative contributions were deduced by subtracting the thermodynamic component from the seasonal evolution of pCO_2.

2.2. Observation Data Sets

In order to evaluate the model behavior against observations, we computed monthly climatologies for surface chlorophyll concentrations and pCO_2. For surface chlorophyll concentrations, we used the surface

chlorophyll distribution from MODIS-Aqua (Moderate Resolution Imaging Spectroradiometer, Standard Mapped Images—Level 3 products) that covers the period 2002–2011 distributed by the Goddard Space Flight Center and reprocessed with an algorithm specifically adapted for the SO (Johnson et al., 2013). For pCO_2, two observation products with different interpolation schemes have been used: the reconstructed monthly maps of surface pCO_2 from Landschützer et al. (2014) and from Takahashi et al. (2009). The first data set (Landschützer et al., 2014) extrapolates observations synthesized in the Surface Ocean Carbon Atlas (SOCAT) version 2 (Bakker et al., 2014) database and covers the period from 1998 to 2011, with a spatial resolution of $1° \times 1°$. A monthly mean climatology centered on the year 2005 was computed to extract the seasonal cycle from the interannual variability. The second data set (Takahashi et al., 2009) is a monthly climatology constructed from about three million measurements of surface oceanic pCO_2 covering the period 1970–2007 at a resolution of 4°(latitude) $\times$ 5°(longitude). pCO_2 values have been corrected for the reference year 2000. To compare the data-based climatologies and the model results, we have computed the seasonal ΔpCO_2 anomalies by subtracting the annual mean value of ΔpCO_2 to the seasonal evolution of ΔpCO_2.

The monthly mean values of ΔpCO_2 and surface chlorophyll concentrations (CHL) from the observations and the model outputs have been averaged over the SO, defined as the entire oceanic region located south of the Sub-Tropical Front (STF). The Antarctic circumpolar current separates the SO into three main zonal regions with distinct hydrographic properties. Thus, for further analysis, we decomposed the SO into three sub-regions defined from north to south as followed: the Sub-Antarctic Zone (SAZ), the Polar Zone (PZ) and the Antarctic Zone (AZ). The boundaries between these regions were computed from the isocontours front definitions proposed by Orsi et al. (1995) for the STF, the Sub-Antarctic Front (SAF) and the Polar Front (PF). The SAZ lies between the STF and the SAF, the PZ between the SAF and the PF and the AZ between the PF and the Antarctic continent.

3. Results

3.1. Validation of the Modeled Iron Distribution in the SO

Biological activity has been demonstrated to be tightly controlled by iron in the SO. As a consequence, a proper representation of the biological pump in this region requires a realistic simulation of the iron distribution. Figure 1 shows a comparison between the iron distributions from a global database constructed by Tagliabue et al. (2012) and as simulated in the CTL experiment.

Even though the sparse data makes the validation of the model particularly difficult at the scale of the SO, a visual inspection at three depth ranges (0–200, 200–1,000, 1,000–5,000 m) shows that globally the model broadly captures the observed iron distribution. The differences between the observations and the model tend to decrease with depth (Figure 1f). In the Pacific Ocean, south east of New Zealand and south of Tasmania, modeled iron concentrations are slightly too high, especially in the mesopelagic domain (200–1,000 m, Figure 1e). Over the Kerguelen Plateau, observed values appear much lower than in the model. In the Atlantic sector of the SO, the model simulates the iron concentrations along the Greenwich meridian, offshore of Argentina and south of the Cape Horn reasonably well. However, simulated iron concentrations are underestimated north of the Antarctic Peninsula and along the transect west of the Greenwich meridian (Figure 1d). Some biases between the model and the observations occur around the Antarctic coast where the model exhibits a significant overestimate of iron, for instance, in the Ross Sea and in the Amundsen Sea (Figure 1d).

Table 1 shows a statistical analysis of the comparison between the modeled and observed iron distributions. The mean iron concentrations simulated in the model over the top 200 m of the ocean are slightly underestimated. In the deep ocean, they are more strongly underestimated, by about 0.1 nmol L^{-1}. The model performs the best in the deep ocean where the correlation coefficient (R) is the highest and the mean absolute error (MAE) is the lowest. In the upper ocean, the model performs less well with a R value of 0.35 and a MAE of 0.34 nmol L^{-1}. The mesopelagic zone is the domain in which the model exhibits the poorest performance at reproducing the observed variance of iron. This analysis of the modeled iron distribution allows us to conclude that the model realistically represents the mean iron concentrations in the three depth domains. Indeed, it displays no significant underestimation or overestimation of iron concentrations in the SO.

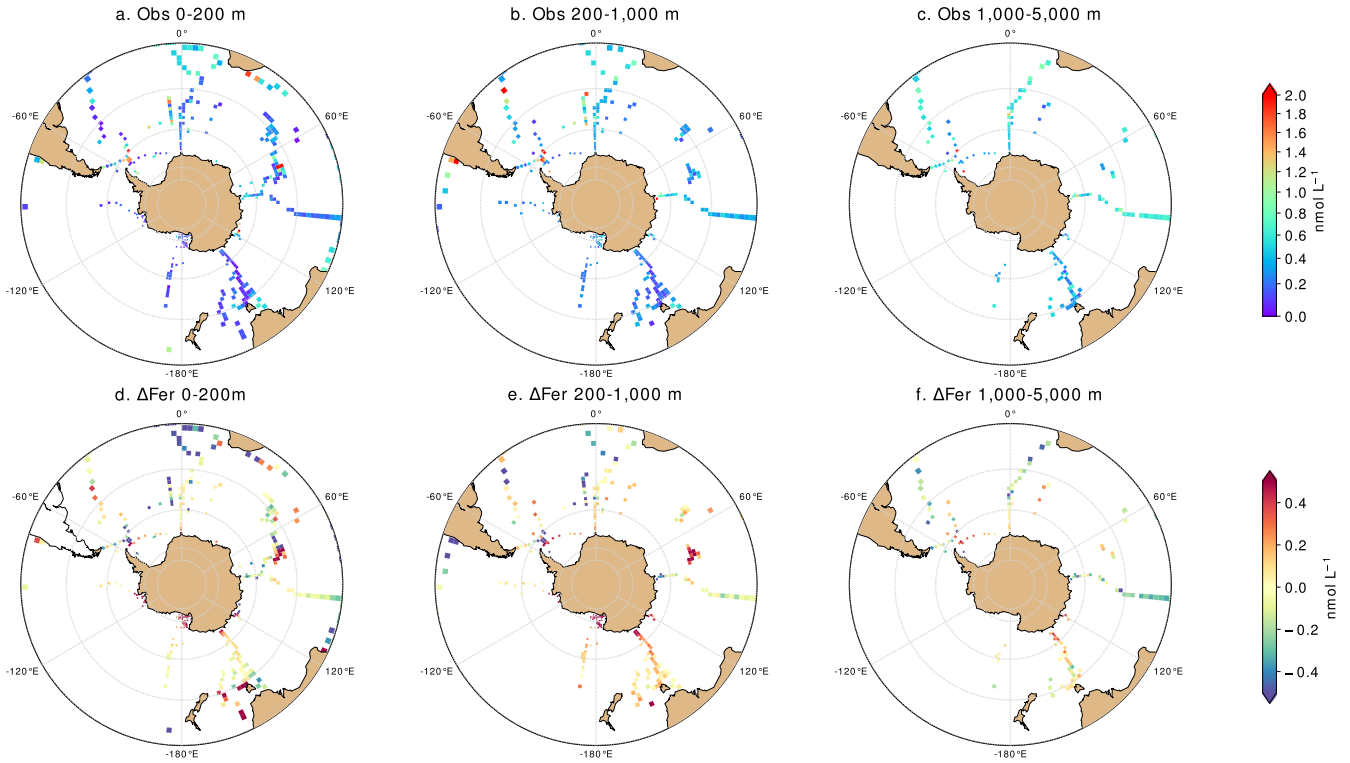

Figure 1. (a–c) Distribution of the mean iron concentrations from observations and (d–f) difference between the mean iron concentrations in the CTL experiment and in the observations in the Southern Ocean, south of 30°S. Iron concentrations are averaged over (a and d) 0–200 m, (b and e) 200–1,000 m and (c and f) 2,000–5,000 m. Model values were sampled at the same location as data.

3.2. An Enhanced Biological Pump Driven by Diatoms Primary Production

The implementation of a low and constant minimum iron quota for diatoms in the biogeochemical model has a noticeable impact on the spatial distribution of the iron quota of diatoms in the SO (Figure 2). In the CTL experiment (Figure 2a), this quota displays summer values ranging from 10 to 25 μmol Fe mol C^{-1} with lower values in the open ocean and higher values in coastal regions such as over the Kerguelen Plateau, near the South Georgia Island and the Crozet archipelago, and close to the Antarctic coast. In the PHYSIO experiment, the model predicts much lower iron quotas for diatoms in the open ocean. These quotas are reduced by a factor of about 2 with mean values around 5 μmol Fe mol C^{-1} (Figure 2b). In coastal regions and downstream of the southern islands, iron quotas remain similar to the values predicted in the CTL experiment. This more contrasted distribution of the diatoms iron quota illustrates the larger plasticity of the iron requirements of this phytoplankton group in the PHYSIO experiment. This higher spatial variability is in agreement with studies on the physiology of diatoms (Kustka et al., 2007; Marchetti et al., 2006; Strzepek & Harrison, 2004), which show large differences in the iron quotas of oceanic and coastal diatom species.

Table 1
Statistical Analysis of the Distribution of Iron in the Southern Ocean, South of 35°S, in the Data and in the CTL Experiment. R is the Correlation Coefficient and MAE, the Mean Absolute Error

	0–200 m		200–1,000 m		1,000–5,000 m	
	Data (n = 1379)	CTL	Data (n = 878)	CTL	Data (n = 582)	CTL
Mean Fer (nmol L^{-1})	0.43	0.40	0.47	0.48	0.58	0.47
R		0.35		0.13		0.46
MAE (nmol L^{-1})		0.34		0.29		0.24

The lower iron requirements of diatoms in the PHYSIO experiment allow this phytoplankton group to become more competitive at low dissolved iron concentrations. This translates into a larger diatoms biomass during the productive season that increases the total primary production in the SO (Table 2). In the CTL experiment, diatoms contribute ∼38% of the total primary production in the SO, ∼32% in the SAZ, ∼35% in the PZ, and ∼45% in the AZ. The new parametrization increases this contribution to ∼48% in the SO, ∼36% in the SAZ, ∼49% in the PZ, and 56% in the AZ. The 10% increase in the diatom contribution to the SO total primary production brings the PHYSIO experiment closer in line with the lower range of estimates from satellite observations that suggest that diatoms contribute from 50% to

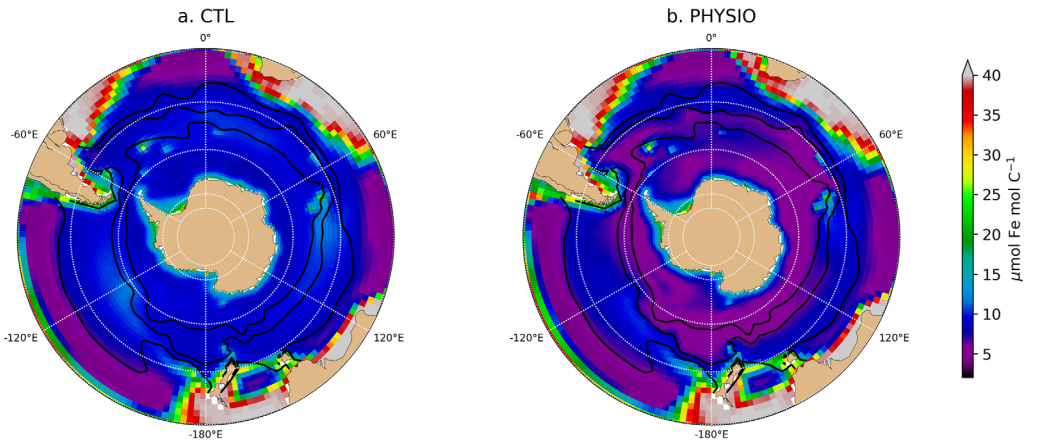

Figure 2. Spatial distribution of the mean iron quota of diatoms in summer (December, January, and February) in the Southern Ocean, south of 30°S in (a) the CTL experiment and (b) the PHYSIO experiment. Annual mean positions of the fronts are shown by the black lines: from north to south, the STF, the SAF, and the PF.

89% to total primary production in the SO (Alvain et al., 2008; Rousseaux & Gregg, 2013). Overall, primary production is increased by 0.244 GtC yr^{-1}, the PZ and the AZ contributing mainly to this increase (Table 2).

Diatoms are known to strongly contribute to carbon export in the SO, but show a variable efficiency (Pollard et al., 2007, 2009; Rembauville et al., 2015; Rigual-Hernández et al., 2015a, 2015b; Salter et al., 2012). Quantifying the carbon export from observations in the SO is a challenging task due to the lack of observations. Thus, a proper evaluation of the model behavior is impossible at the scale of the SO. Here we compare the carbon export at 150 m simulated in our two experiments for the summer period (Figure 3). In both experiments, the spatial distribution of the carbon export over the SO is contrasted. The highest values are found in naturally iron-fertilized regions and the lowest values in open ocean areas that are not downstream of islands (Figures 3a and 3b). The main difference is a significant increase of carbon export in the PHYSIO experiment in regions where export is already low (Figure 3b). These increased values of carbon export remain within the range of observations (Ducklow et al., 2008; Laurenceau-Cornec et al., 2015; Morris et al., 2007; Puigcorbé et al., 2017; Roca-Martí et al., 2017).

Total carbon export in the SO is increased by 16% from 1.47 GtC yr^{-1} in the CTL experiment to 1.71 GtC yr^{-1} in the PHYSIO experiment (Table 3). Although the diatom contribution to total primary production is increased by 10% (Table 2), the larger relative increase in export is explained by the more efficient carbon export out of the euphotic zone sustained by diatoms. However, this change in export exhibits distinctive differences between the three hydrological provinces (Table 3). The SAZ, which has the largest contribution to carbon export in the CTL experiment with 0.59 GtC yr^{-1}, shows the lowest increase of about 0.02 GtC yr^{-1}, i.e. 3%, in the PHYSIO experiment. In the PZ and the AZ, carbon export is increased by 0.08 GtC yr^{-1} and by 0.12 GtC yr^{-1} respectively, which represents an increase of 23%. With the new parametrization, the AZ becomes the region where carbon export is the largest.

Table 2
Relative Contribution of Diatoms to Total Primary Production in the CTL and PHYSIO Experiments. The Difference in Total Primary Production Integrated Over Depth Between the PHYSIO and the CTL Experiments (ΔPP in GtC yr^{-1}) Is Also Shown for the Sub-Antarctic Zone (SAZ), the Polar Zone (PZ), the Antarctic Zone (AZ) and the Southern Ocean (SO), South of the Subtropical Front. In Brackets Are the Values of the Total Primary Production Integrated Over Depth in the CTL Experiment

Experiment	SAZ	PZ	AZ	SO
CTL	32%	35%	45%	38%
PHYSIO	36%	49%	56%	48%
ΔPP (GtC yr^{-1})	0.026 (2.1)	0.097(1.3)	0.120 (1.7)	0.244 (5.5)

3.3. Spatial Distribution of Surface Chlorophyll

First, we analyze the ability of the model to reproduce the spatial patterns of CHL during the most productive season (December, January, and February) in the SO, south of 30°S. Qualitatively, the comparison between the observations and the CTL experiment shows that the model reproduces the specific HNLC distribution of CHL in the whole SO with large areas characterized by low values that contrast with specific regions of high CHL (Figures 4a and 4b). The model captures the island mass effect, which initiates blooms downstream of Kerguelen Island and associated plateau, the Crozet Islands and the South Georgia Island (Sullivan et al., 1993; Tyrrell et al., 2005). These naturally iron-fertilized regions (Blain et al., 2007; Borrione & Schlitzer, 2013; Pollard et al., 2007) are represented in the model thanks to the inclusion of specific coastal and shelf iron sources. Along the Antarctic coast,

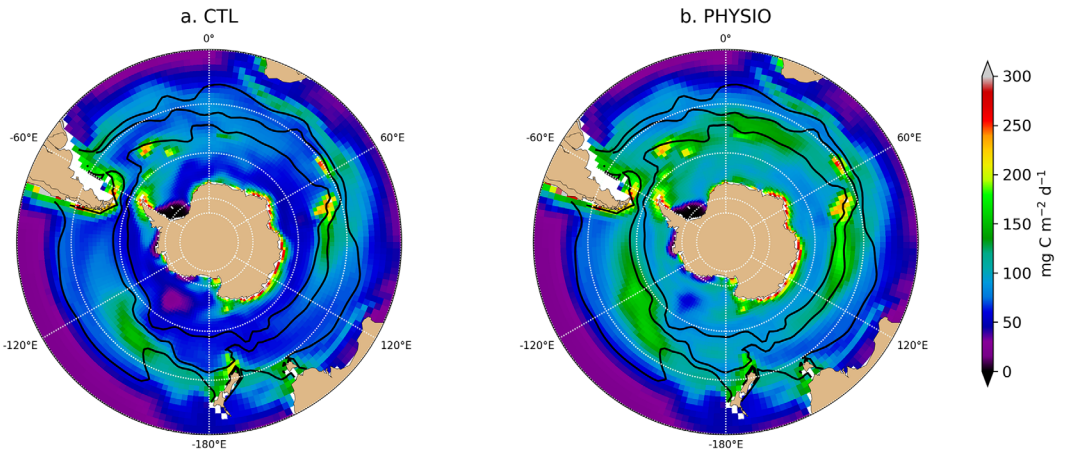

Figure 3. Spatial distribution of the mean carbon export at 150 m (mgC m^{-2} d^{-1}) in summer (December, January, and February) in (a) the CTL experiment and (b) the PHYSIO experiment. Annual mean positions of the fronts are shown by the black lines: from north to south, the STF, the SAF, and the PF.

the model predicts a summer bloom of CHL which displays the correct magnitude but observations show more contrasted spatial distributions (Figure 4a). The most notable biases occur mainly in the frontal zone between the STZ and the SAZ, north of 45°S, along the Patagonian shelf, in the region of the Agulhas current retroflection and around New Zealand. The resolution of the model is too coarse to represent the nutrient enrichment induced by the elevated mesoscale and submesoscale activities that characterize these regions (Lévy et al., 2012; Rosso et al., 2015, 2016).

The new parametrization is not expected to improve the spatial distribution of CHL (Figure 3c) since these patterns are strongly driven by dynamical and topographical features (Mashayek et al., 2017; Rosso et al., 2015), which are identical in both runs. However, some slight improvements are displayed in the PHYSIO experiment as supported by a quantitative evaluation of the model experiments presented in Table 4 and comprising the correlation coefficient (R), the mean absolute error (MAE), the average error (AE) and the normalized standard deviation (STD). Two other model performance metrics are added to assess the model skill as suggested in Stow et al. (2009): the reliability index (RI) (Leggett & Williams, 1981) and the modeling efficiency (MEF) (Nash & Sutcliffe, 1970). The RI denotes the average factor by which the model diverges from the observations. This index should be close to 1. The MEF evaluates how well the model predicts observations relative to the average of the observations. A value near 1 indicates a close match with the observations. A negative value means that the average of the observations is a better predictor than the model. For CHL, the scores for MAE, AE, STD and MEF are almost identical in both runs. Nonetheless, moderate improvements are displayed in the PHYSIO experiment, the coefficient of correlation showing a slightly higher value than in the CTL experiment and the RI index decreasing to a value closer to 1.

3.4. Seasonal Evolution of Surface Chlorophyll

Here we analyze to which extent the lower iron requirement of diatoms modifies the modeled representation of the seasonal cycle of CHL. While the new parametrization only modestly improves the skill of the model to reproduce the spatial distribution of CHL in the SO, the seasonal evolution of CHL exhibits a better agreement with the observations than in the CTL experiment (Figure 5d). In particular, the PHYSIO experiment predicts a larger seasonal cycle amplitude in CHL, with a peak value of the bloom in December that is almost identical to the observed climatological value. The decline of the bloom from December to May also shows a temporal evolution which follows more closely the observations but with mean CHL values about 0.1 mg m^{-3} too low from January to May.

This global improvement in the seasonal evolution of CHL with the new parametrization conceals contrasted results in the three hydrological provinces. In the SAZ (Figure 5a), both experiments simulate

Table 3
Annual Mean Carbon Export at 150 m in GtC yr^{-1} in the CTL and the PHYSIO Experiments in the Sub-Antarctic Zone (SAZ), the Polar Zone (PZ), the Antarctic Zone (AZ), and the Southern Ocean (SO), South of the Subtropical Front

Experiment	SAZ	PZ	AZ	SO
CTL	0.59	0.35	0.53	1.47
PHYSIO	0.61	0.43	0.65	1.71

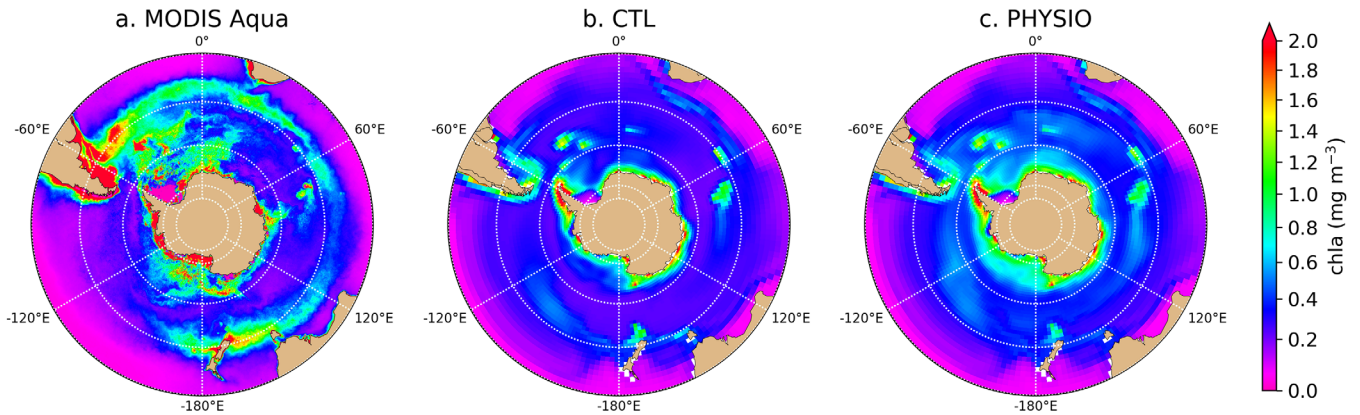

Figure 4. Spatial distribution of the mean surface chlorophyll concentrations in summer (December, January, and February) in the Southern Ocean, south of 30°S, from (a) observations (MODIS-Aqua), (b) the CTL experiment, and (c) the PHYSIO experiment. Annual mean positions of the fronts in the model are shown in both experiments by the black lines: from north to south, the STF, the SAF, and the PF.

relatively similar variations of CHL. Nonetheless, in the PHYSIO experiment, the bloom peaks about one month later, in December, and CHL concentrations remain slightly higher from January to March. This seasonal evolution agrees slightly better with satellite observations, even if the summer mean values remain underestimated by 0.07 mg Chl m^{-3}. In the PZ (Figure 5b), the CHL seasonal cycle simulated in the PHYSIO experiment is notably improved with a summer peak bloom in December instead of November in the CTL experiment. The amplitude of the bloom is also strongly increased although underestimated by about 0.1 mg Chl m^{-3} compared with the observations. The decline of the bloom from December to May shows higher values during the whole period in better agreement with the observations. In the AZ (Figure 5c), the PHYSIO experiment also predicts a larger seasonal cycle than in the CTL experiment. Relative to the satellite data, the bloom onset, its development and its decline are in phase with the observations. The peak of the bloom arises one month too early in December, while CHL is slightly overestimated by about 0.05 mg Chl m^{-3}.

3.5. Spatial Distribution of ΔpCO_2

We found that parametrizing the physiological adaptation of SO diatoms to the low availability of iron increased primary production and strengthened the efficiency of the biological pump in the SO. In this section, we attempt to quantify the consequences of the enhanced biological pump on the air-sea CO_2 exchange by examining the seasonal variability of pCO_2.

Figure 6 shows the spatial distributions of the seasonal amplitude (winter minus summer) of ΔpCO_2 in the two data-based climatologies and in both model experiments. The observations display an annular distribution of negative and positive seasonal differences of ΔpCO_2 in the SO with high positive values around the Antarctic continent, lower positive values ranging from 0 to 40 μatm from 60°S to 45°S and negative values north of 40°S (Figures 6a and 6b). The positive annular distribution around the Antarctic continent is properly represented in both experiments as well as the negative annular difference north of 40°S. The main change lies between 40°S and 60°S where the CTL experiment simulates an alternating longitudinal distribution of positive and negative seasonal differences of ΔpCO_2. Large areas of negative values are found in the Atlantic basin, north of the South Georgia Island, in the Indian basin, south of the Kerguelen Plateau, and in the Pacific sector, south of New Zealand (Figure 6c). These large regions of negative values, which fall in a zonal band that encompasses the PZ and the northern part of the AZ, are absent in both data-based climatologies (Figures 6a and 6b). The PHYSIO experiment seems to partly correct this bias by reducing the magnitude of the negative seasonal differences south and north of the PF (Figure 6d).

Table 4
Statistical Model-Data Comparison of the Two Experiments for Surface Chlorophyll Concentrations South of the STF. R, MAE, AE, STD, RI, and MEF are, Respectively, the Correlation Coefficient, the Mean Absolute Error, the Average Error, the Normalized Standard Deviation, the Reliability Index, and the Modeling Efficiency

	CTL	PHYSIO
R (log)	0.51	0.53
MAE (mg Chl m^{-3})	0.29	0.27
AE (mg Chl m^{-3})	−0.27	−0.23
STD	0.25	0.22
RI	2.06	1.89
MEF	−0.01	0.03

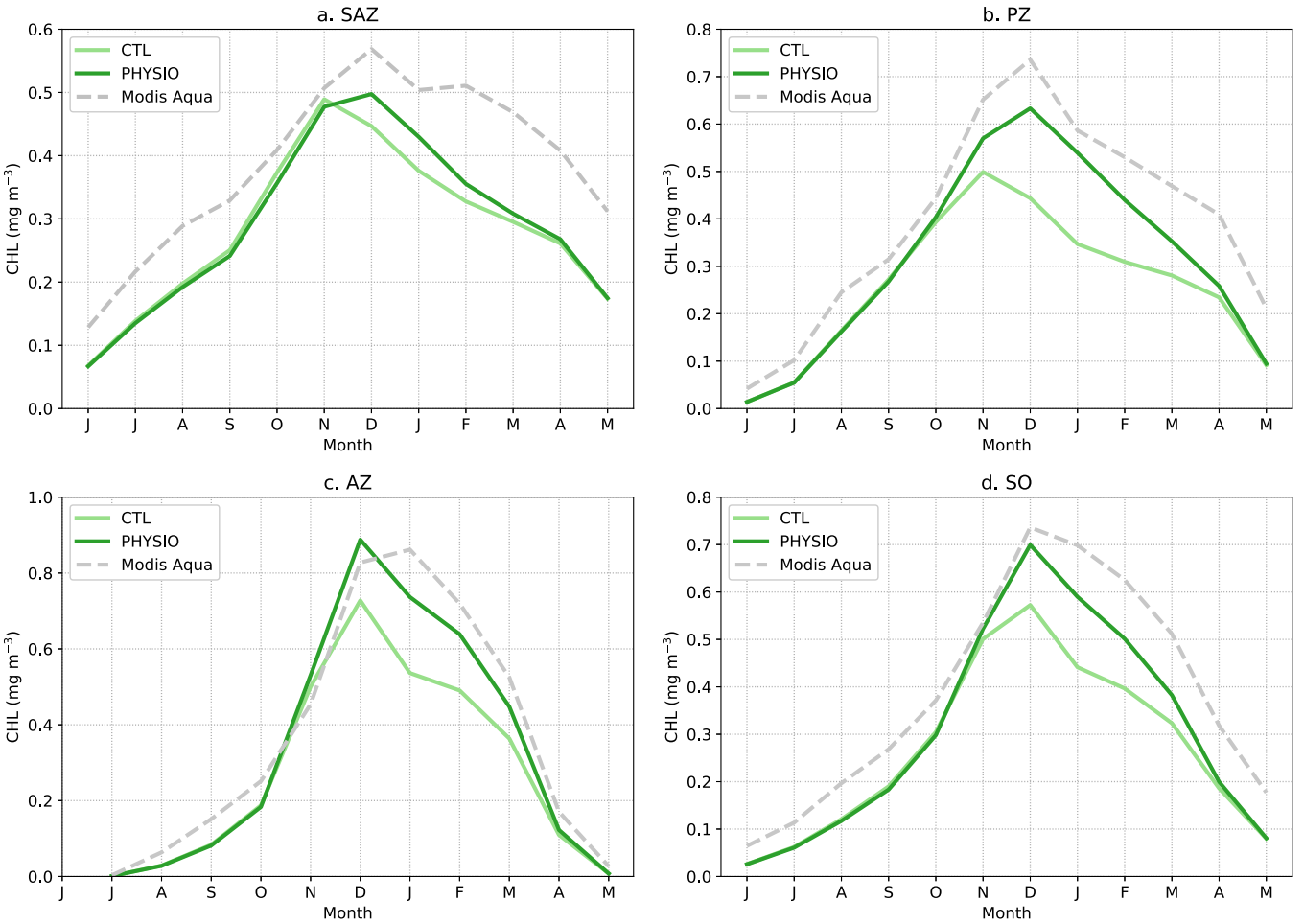

Figure 5. Seasonal cycles from June to May of the surface chlorophyll concentrations (mg Chl m^{-3}) from the remote sensing observations (dashed line, gray), the CTL experiment (light green), and the PHYSIO experiment (dark green) averaged over (a) the Sub-Antarctic Zone (SAZ), (b) the Polar Zone (PZ), (c) the Antarctic Zone (AZ), and (d) the Southern Ocean (SO), south of the subtropical front.

The statistical analyzes of the spatial distribution of the ΔpCO_2 anomalies between the data-based product of Landschützer et al. (2014) and the experiments provide a more quantitative evaluation of the model behavior. Over the SO, the scores of the PHYSIO experiment show no marked improvements compared to the CTL experiment (Table 5). The correlation coefficients are equal, and the MAE and the RI index are almost identical in both experiments. The AE is improved since it is closer to zero whereas both the STD and the MEF exhibit a poorer performance in the PHYSIO experiment. However, when this statistical analysis is restricted to both the SAZ and the PZ, the scores of the PHYSIO experiment are now notably improved compared to the CTL experiment. The slightly higher value of R suggests that the spatial patterns of ΔpCO_2 are better simulated than in the CTL experiment. Biases between predicted and observed values of ΔpCO_2 anomalies are markedly reduced in the PHYSIO experiment as illustrated by the lower values of both MAE and AE. Furthermore, the normalized standard deviation is slightly closer to 1. Finally, the PHYSIO experiment exhibits better model performance with a slightly lower and closer to 1 RI index and a MEF index that switches from a significantly negative value in the CTL experiment to a positive value in the PHYSIO experiment. This statistical analysis together with the qualitative comparison between the spatial distributions of ΔpCO_2 suggest that the region located in the southern part of the AZ, i.e., in the seasonally ice-covered zone, seems to introduce significant biases in the spatial distribution of ΔpCO_2 in the model. The lower iron requirement of diatoms prescribed in the PHYSIO experiment appears to increase this bias. This conclusion is further illustrated in the following description of the seasonal cycle of ΔpCO_2.

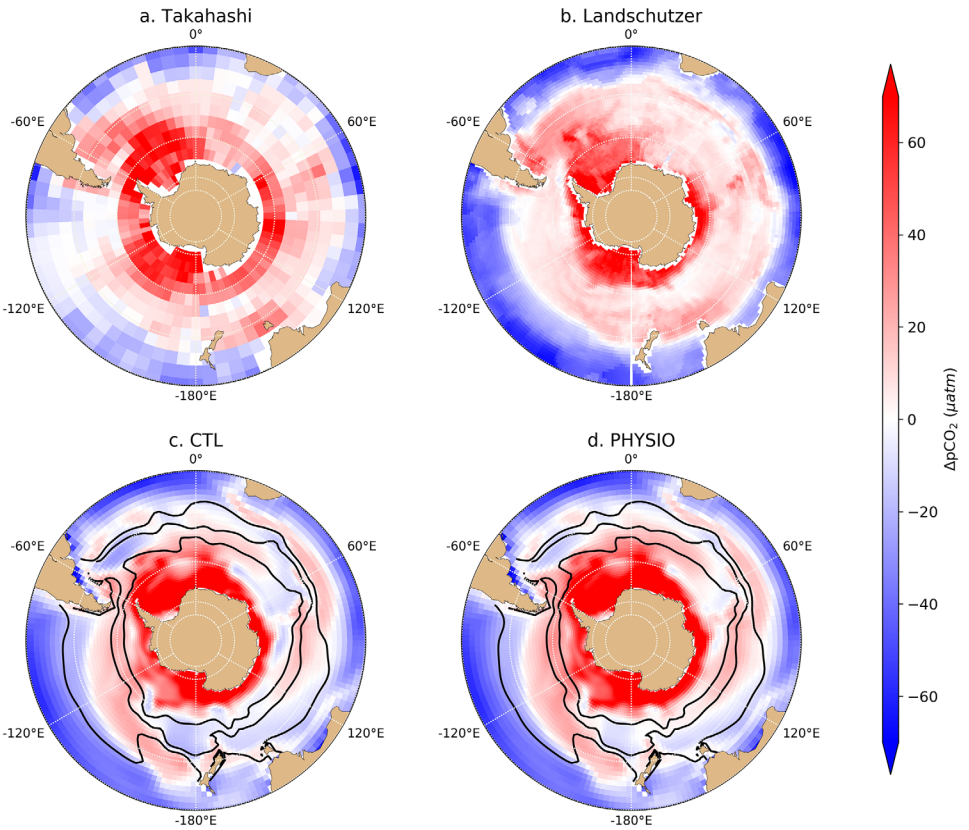

Figure 6. Spatial distribution of the seasonal amplitude (winter minus summer) of ΔpCO_2 ($pCO_2^{oc} - pCO_2^{atm}$) determined from (a) the Takahashi climatology, (b) the Landschützer climatology, (c) the CTL experiment, and (d) the PHYSIO experiment. Winter encompasses June, July, and August and summer December, January, and February. Annual mean positions of the fronts in the model are shown in both experiments (black lines): from north to south, the STF, the SAF, and the PF.

3.6. Seasonal Evolution of ΔpCO_2

The phasing of the seasonal evolution of ΔpCO_2 averaged over the SO is slightly modified when the physiological adaptation of diatoms is introduced in the model (Figure 7d). Maximum values of ΔpCO_2 in the PHYSIO experiment are reached in September as shown by the observations. Minimum values are reached one month later than in the CTL experiment, in January, in agreement with the observations. In the PHYSIO experiment, the seasonal amplitude is increased by about 6 μatm which seems to be too large, whereas the amplitude simulated in the CTL experiment falls within the lower range of the data-based climatologies.

Table 5
Statistical Model-Data Comparison of the Two Experiments for ΔpCO_2 ($pCO_2^{oc} - pCO_2^{atm}$) Anomalies in the Southern Ocean (SO) and in the Region That Encompasses the SAZ and the PZ (SAZ + PZ), South of the STF. R, MAE, AE, STD, RI, and MEF are, Respectively, the Correlation Coefficient, the Mean Absolute Error, the Average Error, the Normalized Standard Deviation, the Reliability Index, and the Modeling Efficiency

	SO		SAZ + PZ	
	CTL	PHYSIO	CTL	PHYSIO
R	0.67	0.67	0.43	0.49
MAE (μatm)	10.9	11.3	7.08	6.40
AE (μatm)	3.16	−1.75	4.27	2.21
STD	1.20	1.42	0.85	0.89
RI	1.47	1.43	1.67	1.61
MEF	0.15	−0.13	−0.24	0.02

The observed ΔpCO_2 seasonal cycle in the SAZ (Figure 7a) is characterized by a double peak which is representative of a transition between the oligotrophic warm waters of the subtropics, north of the SAZ, and the more productive waters, south of the SAZ (Merlivat et al., 2015; Metzl, 2009). The summer peak ensues from the warming of surface waters (solubility effect) whereas the winter maximum results from the vertical entrainment of subsurface DIC-rich waters. In the PHYSIO experiment, the summer peak is lower, and the winter peak is slightly higher than for the CTL experiment. This marks a shift to a regime in which the vertical entrainment of nutrients in winter and the biological pump in summer exert a stronger control on pCO_2. This interpretation is supported by the decomposition of ΔpCO_2 into its thermal component which is a function of sea surface temperature (SST) and into its both biological and dynamical components (Figure 8a). The

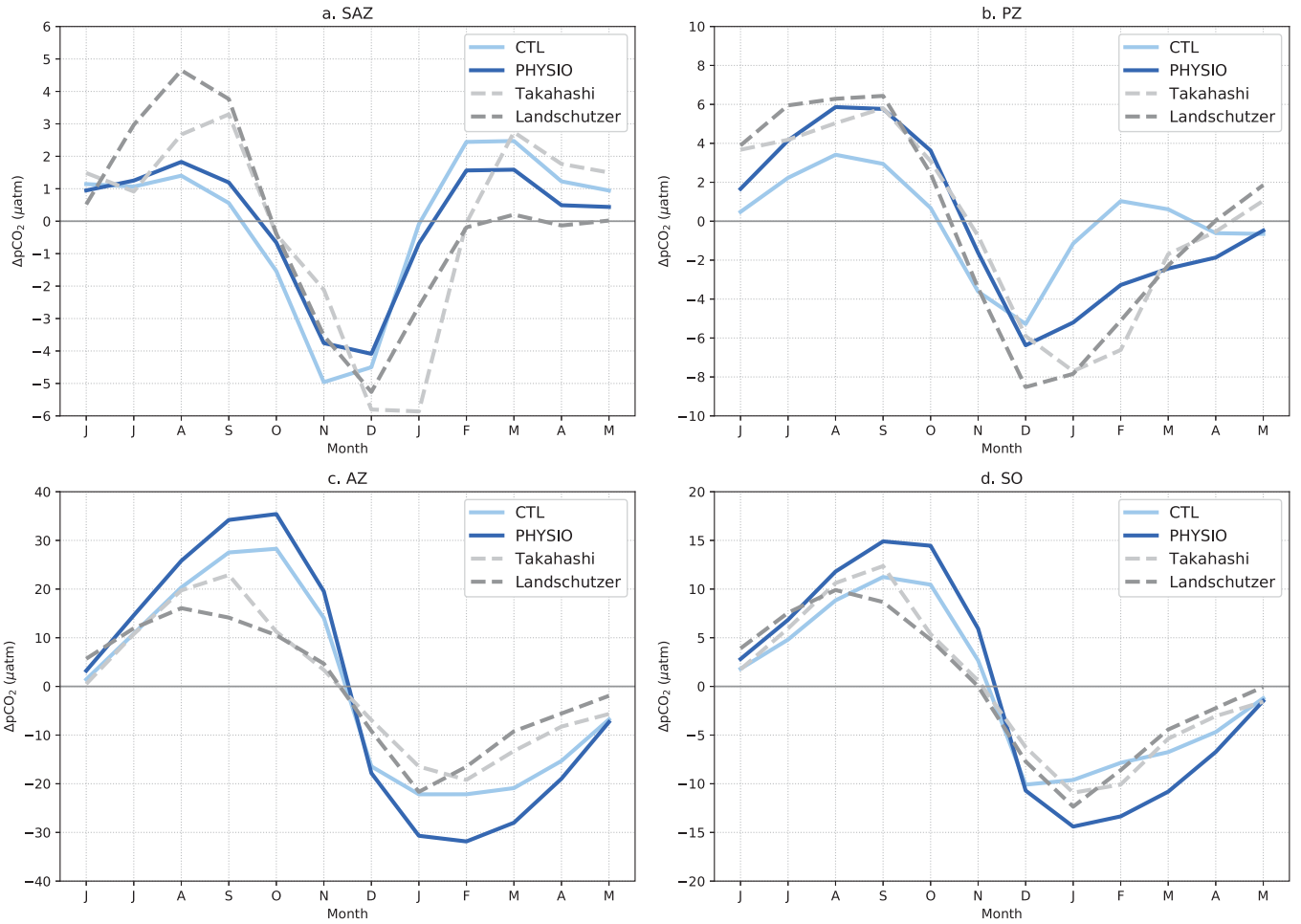

Figure 7. Seasonal cycles from June to May of the anomalies of ΔpCO_2 ($pCO_2^{oc} - pCO_2^{atm}$) from observations, Landschützer data set (dashed line, dark gray), Takahashi data set (dashed line, light gray), the CTL experiment (light blue), and the PHYSIO experiment (dark blue) averaged over (a) the Sub-Antarctic Zone (SAZ), (b) the Polar Zone (PZ), (c) the Antarctic Zone (AZ), and (d) the Southern Ocean (SO), south of the subtropical front.

thermal contribution shows no difference between both experiments whereas the dynamical and biological contributions to the seasonal evolution of pCO_2 are slightly increased in the PHYSIO experiment. However, this shift is too weak to cancel out the model deficiencies in that region which suggests that the biological pump remains on average too weak in the PHYSIO experiment.

In the PZ, the phase and the amplitude of the seasonal cycle of ΔpCO_2 simulated in the PHYSIO experiment are closer to the observations than in the CTL experiment (Figure 7b). The CTL experiment simulates a seasonal cycle characterized by two low maximums in August and February. This strongly contrasts with the observations which exhibit a minimum in summer followed by a single maximum in winter. This erroneous double peak disappears in the PHYSIO experiment where the seasonal amplitude is larger, the maximum being reached in August and the minimum in December in agreement with the observations. The ΔpCO_2 seasonal cycle amplitude in the PHYSIO experiment remains too low by 2 μatm.

In the PHYSIO experiment, the longer and stronger bloom induces a more intense DIC uptake through photosynthesis than in the CTL experiment. This larger uptake is associated with a larger carbon export, driving a stronger vertical gradient of DIC (Figure 9a). During this productive season (between December and February), warmer temperatures act to increase oceanic pCO_2. This thermodynamic effect is balanced by the biological uptake of DIC that tends to decrease surface pCO_2. In the PHYSIO experiment, the biological effect is stronger than the thermodynamic effect, leading to a decrease in pCO_2 (Figure 8b). In the CTL experiment, a similar thermodynamic effect associated to a weaker biological uptake results in a small increase in pCO_2. In winter (from June to October), the solubility effect is equal in both experiments.

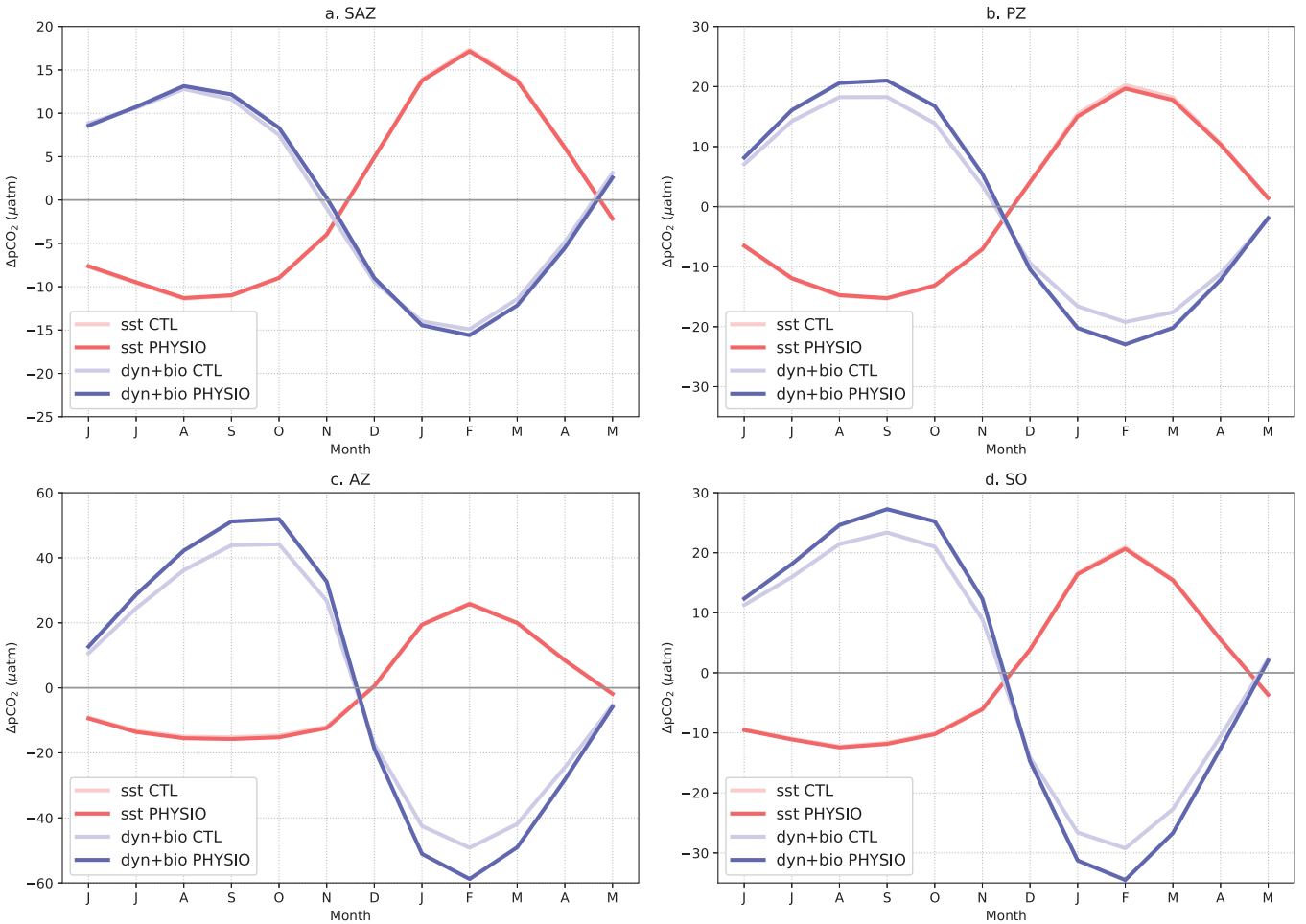

Figure 8. Seasonal cycles from June to May of the thermodynamical (sst) and both biological and dynamical (dyn + bio) relative contributions to the seasonal cycle of ΔpCO_2 averaged over (a) the Sub-Antarctic Zone (SAZ), (b) the Polar Zone (PZ), (c) the Antarctic Zone (AZ), and (d) the Southern Ocean (SO), south of the subtropical front. The light red (CTL) and the dark red (PHYSIO) curves denote the thermodynamic effect. The biological and physical factors are displayed in light blue (CTL) and dark blue (PHYSIO).

However, the winter entrainment of DIC is stronger in the PHYSIO experiment leading to a larger increase in pCO_2 in September, about 3 µatm more than in the CTL experiment. The larger amplitude of the seasonal cycle of ΔpCO_2 in the PHYSIO experiment compared to the CTL experiment is thus due to a larger

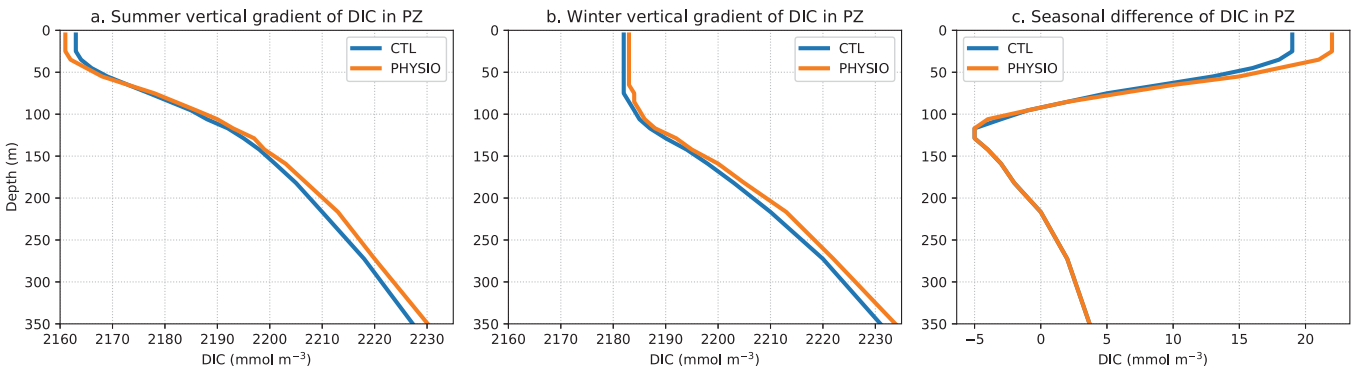

Figure 9. Vertical gradients of DIC (mmol m^{-3}) from 0 to 350 m depth in (a) summer, (b) winter, and (c) seasonal difference (winter minus summer) of the vertical gradients of DIC in the CTL experiment (blue) and in the PHYSIO experiment (orange) in the Polar Zone.

contribution of both the biological uptake (around 4 μatm in summer) and the physical supply of DIC (around 3 μatm in winter).

This result is illustrated in Figure 9 that shows vertical profiles of DIC in the upper layer. These profiles are almost identical in winter in both experiments (Figure 9b) whereas the vertical gradient of DIC in summer is larger in the PHYSIO experiment (Figure 9a). In comparison with the CTL experiment, summer DIC concentrations in the PHYSIO experiment are lower in the mixed layer and higher below. This difference intensifies the amplitude of the seasonal gradient (winter minus summer) of DIC in the mixed layer in the PHYSIO experiment (Figure 9c) suggesting that the biological pump may drive a part of the winter entrainment of DIC.

In the AZ (Figure 7d), the seasonal amplitude of ΔpCO_2 simulated in the CTL experiment is on average 25% larger than in the climatologies of Takahashi et al. (2009) and Landschützer et al. (2014). The PHYSIO experiment amplifies this bias by increasing this amplitude by 30% suggesting that the biological drawdown of DIC during the favorable season is much too large (Figure 8d). However, in the latter, the seasonal variations of surface chlorophyll fall within the range of the observations (Figure 5c). Yet, the AZ is characterized by a high biomass low export regime (Lam & Bishop, 2007), thus a potential explanation for these apparently contradicting features is that the model predicts a realistic magnitude of primary productivity, but a too efficient carbon export to the ocean interior. Indeed, it has been suggested that the SO is characterized by a low vertical transfer efficiency of export, whose causes remain elusive (Cavan et al., 2015; Laurenceau-Cornec et al., 2015; Le Moigne et al., 2016; Maiti et al., 2013; Morris et al., 2007).

3.7. Sea-Air CO_2 Flux

Figure 10a shows the annual mean sea-air fluxes of CO_2 for 2010, for the three hydrological provinces and for the whole SO. Observations and modeled integrated fluxes are computed using the formulation of the gas transfer coefficient proposed by Wanninkhof (1992). Taking into account the physiological adaptation of diatoms to low iron increases the biological pump, which then has a moderate, but nonnegligible impact on the integrated sea-air CO_2 flux in each zone (Figure 10a). The stronger carbon export in the PHYSIO experiment enhances the carbon pump in the SAZ and in the PZ relative to the CTL experiment. In both regions, the total annual uptake of CO_2 is slightly increased (by 0.04 and 0.05 PgC yr^{-1} in the SAZ and in the PZ, respectively). The model better matches the observational estimates in the SAZ, and switches from a slight source to a slight sink of atmospheric CO_2 in the PZ as suggested from data-based flux estimates. However, these results are not statistically significant as they remain within the $\pm$0.15 PgC yr^{-1} observational uncertainty range. The main discrepancy between the model experiments and the observations occurs in the AZ. The sea to air outgassing of carbon is much larger than estimated from the observations, more than 10 times larger in both experiments. The new parametrization does not improve the model performance, and in fact even slightly worsens it. The increased degassing of carbon to the atmosphere in the AZ in the PHYSIO experiment is explained by the stronger export of DIC to the deep ocean in the SAZ and

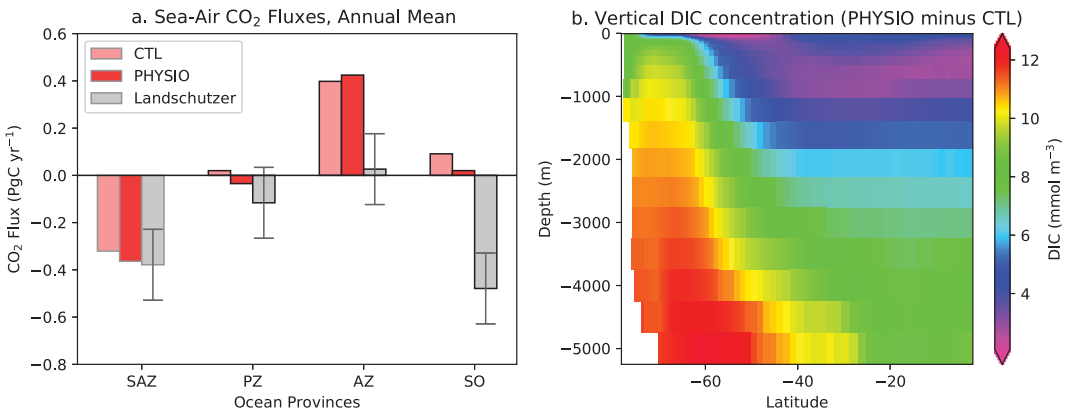

Figure 10. (a) Annual mean sea-air fluxes of CO_2 (PgC yr^{-1}) integrated over the SO and over the three provinces in the CTL experiment (pink), the PHYSIO experiment (red), and the observations (gray) for 2010. Error bars in the observations are overprinted in dark gray. (b) Difference in the zonal mean concentrations of DIC (mmol m^{-3}) between both experiments (PHYSIO minus CTL).

in the PZ. The resulting larger concentrations of DIC in the ocean's interior are transported back to the surface in the AZ by upwelling and deep convective mixing (Figure 10b). Finally, the sea-air CO_2 flux estimated from the PHYSIO experiment over the SO is still a slight source of CO_2 for the atmosphere mainly due to the biased representation of the carbon source in the AZ, at least with respect to the data-based climatologies.

4. Discussion

This sensitivity study shows that taking into account the adaptive strategy of diatoms to low iron concentrations in the SO has significant impacts on the representation of the biological pump and the seasonal evolution of surface chlorophyll and pCO_2 in this region. The contribution of the biological pump to the air-sea CO_2 exchange is increased, which substantially alters the subtle balance between the simulated biological, dynamical and thermodynamic factors that shape the seasonal variability of pCO_2. In the specific case of PISCES, this tends to better reconcile the model with the observed seasonal variability of CHL in the whole SO and, at least partially, the seasonal evolution of pCO_2, mainly in the PZ. A high primary production associated with a weak vertical mixing in the upper ocean drives pCO_2 to low values during summer whereas low winter primary production and intense mixing in winter cause high pCO_2 values, counterbalancing the solubility effect. In addition, our model experiments suggest that the winter entrainment of carbon is tightly coupled to the biological export of carbon in summer, with increased carbon export leading to increased entrainment of DIC.

Our results point to a discrepancy in the seasonal cycle of pCO_2 between the observations and the model in the AZ where the model strongly overestimates the amplitude of the seasonal variations of pCO_2 (Figure 7c). The data coverage in autumn and winter in this region is particularly scarce and is not sufficient to fully constrain the winter end member of the seasonal cycle (Bakker et al., 2014). Moreover, the spatial distribution of pCO_2 provided by the data-based climatologies are constructed by large scale interpolation of sparse observations in space and have strong temporal biases. As a consequence the observed seasonal cycle should be considered with care, especially during the unfavorable season. Indeed, the recent study by Williams et al. (2017) shows that the amplitude of the seasonal cycle of pCO_2 might be largely underestimated in the AZ, in agreement with our model. The SOCCOM project (http://soccom.princeton.edu/) will help to fill the gaps in the observations at the seasonal scale in the SO.

Both model experiments display a strong bias when assessing the sea-air CO_2 fluxes in the AZ that shows a large and excessive outgassing of CO_2 compared to the observations (Figure 10a). It is difficult to diagnose if this large error is due to a deficiency in the model behavior or if it arises from a biased estimation due to sparse air-sea CO_2 exchanges observations in the AZ. However, in the model, this bias could be possibly linked to a too strong convection in winter in the SO, especially in the Weddell Sea, which brings back excessive amounts of DIC to the surface.

4.1. Is the Change in the Diatoms Contribution to Total Primary Production Realistic?

Our study links the physiological adaptation of SO diatoms to the intensity of the biological pump through the increased contribution of this phytoplankton group to total primary production in the SO. Quantitatively, the new parametrization increases this contribution by 10% in the whole SO (Table 2). Is this change in the diatoms contribution to total primary production realistic? This is a challenging question in view of the poor data coverage of diatom abundance in the SO. We propose an indirect diagnostic in order to evaluate whether the modeled diatom abundance and silicification in the SO are improved with the new adaptation process. Diatoms synthesize their silica walls or frustules (Round et al., 1990), which are made of hydrated glass (Drum & Gordon, 2003), from silica dissolved in seawater (Armbrust, 2009). They exert a major control on the biogeochemical cycle of silicon in the oceans (Armbrust, 2009; Tréguer & De La Rocha, 2013) and in the SO (Buesseler et al., 2001; Quéguiner & Brzezinski, 2002). Hence, we compared the seasonal cycles of surface silicate predicted by both experiments to the climatology from the World Ocean Atlas. It should be borne in mind that this does not constitute a typical model validation, but a partial and indirect verification of our model. For instance, the seasonal evolution of silicate is not only controlled by the abundance of diatoms but also by their level of silicification (their Si:C ratio), which can be highly variable (Lasbleiz et al., 2014; Martin-Jézéquel et al., 2000; Sarthou et al., 2005) depending on the growing conditions this group experiences (Brzezinski, 1985; Bucciarelli et al., 2010; Hoffmann et al., 2007; Lasbleiz et al., 2014). We find that the seasonal evolution of surface silicate concentrations (Si) in the PHYSIO experiment is

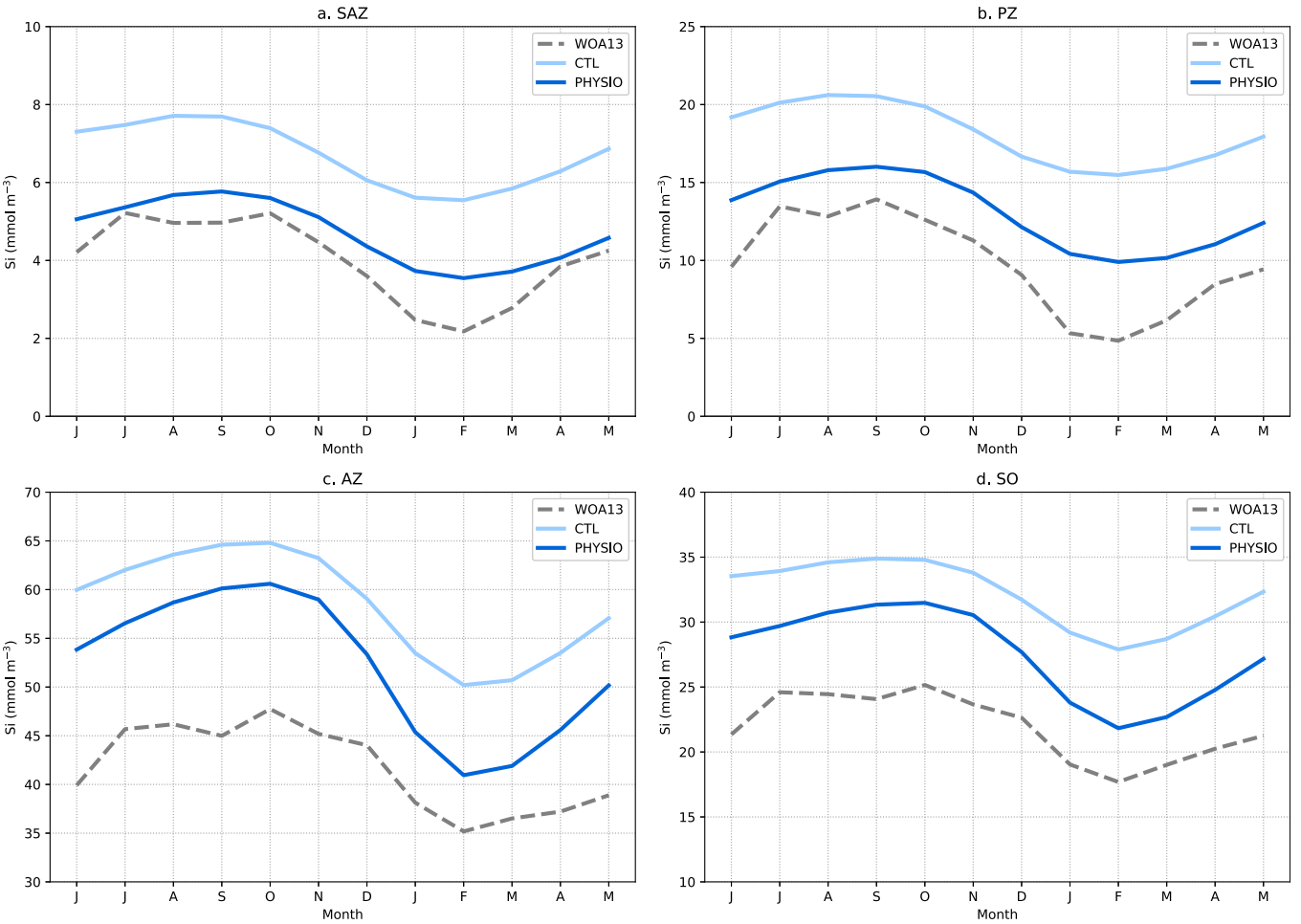

Figure 11. Seasonal cycles from June to May of the surface silicate concentration (Si, mmol m^{-3}) from the World Ocean Atlas 2013 observations climatology (dashed line, gray), the CTL experiment (light blue), and the PHYSIO experiment (dark blue) averaged over (a) the Sub-Antarctic Zone (SAZ), (b) the Polar Zone (PZ), (c) the Antarctic Zone, and (d) the Southern Ocean (SO), south of the subtropical front.

improved when compared to climatological data in two hydrological provinces (Figures 11a and 11b). The PHYSIO experiment better reproduces the amplitude and the mean values of Si in the SAZ (Figure 11a) and in the PZ (Figure 11b). In these provinces, the seasonal amplitude simulated in both experiments is weaker than in the observations but displays a slight increase in the PHYSIO experiment. In the AZ, the PHYSIO experiment values range between the CTL experiment and the observations displaying a larger seasonal amplitude (Figure 11c). Both experiments overestimate the observed seasonal evolution of Si in this hydrological province. In the whole SO, the mean value of Si simulated in the PHYSIO experiment stays closer to the observations with a larger amplitude due to the AZ bias (Figure 11d). Quantitatively, this seasonal improvement is supported by the statistical evaluation of the model experiments (Table 6). The correlation coefficient R for both experiments are equal with a mean value of 0.89 indicating that the spatial patterns of Si are not significantly changed between the two model experiments. However, the MAE and AE, which measure the discrepancies between predicted and observed values, are improved in the PHYSIO experiment. The two added indices, RI and MEF, with values closer to 1, denote that the PHYSIO experiment performs better than the CTL experiment. This statistical model-data comparison for Si tends to strengthen the fact that diatom productivity is better represented in the PHYSIO experiment.

Table 6
Statistical Model-Data Comparison of the Two Experiments for the Surface Silicate Concentration South of 35°S. R, MAE, AE, RI, and MEF Are, Respectively, the Correlation Coefficient, the Mean Absolute Error, the Average Error, the Reliability Index, and the Modeling Efficiency

	CTL	PHYSIO
R	0.89	0.89
MAE (mmol m^{-3})	9.70	7.60
AE (mmol m^{-3})	7.70	4.06
RI	2.72	2.37
MEF	0.48	0.61

4.2. Are We Correcting the Right Process? A Mechanistic Assessment of the Model

In the specific case of our model, the explicit representation of the adaptation strategy of diatoms improves the representation of the seasonal evolution of pCO_2, except perhaps for the SAZ. Even if this improvement was not intended as the primary objective of this study, we further analyze here its soundness. As the mean seasonal cycle of pCO_2 is a relatively small residual between two major compensating mechanisms, i.e., the thermally driven solubility changes and the DIC-driven changes, a moderate error in the seasonal cycle of temperature, salinity or entrainment in the model could explain the failure of the CTL experiment at reproducing the correct seasonality of pCO_2. Even though our study focuses on the sensitivity of the carbon cycle to a biological process, here we present arguments to strengthen the point that the incorrect seasonality of pCO_2 in the CTL experiment is mainly explained by the underestimation of the biological drawdown of DIC.

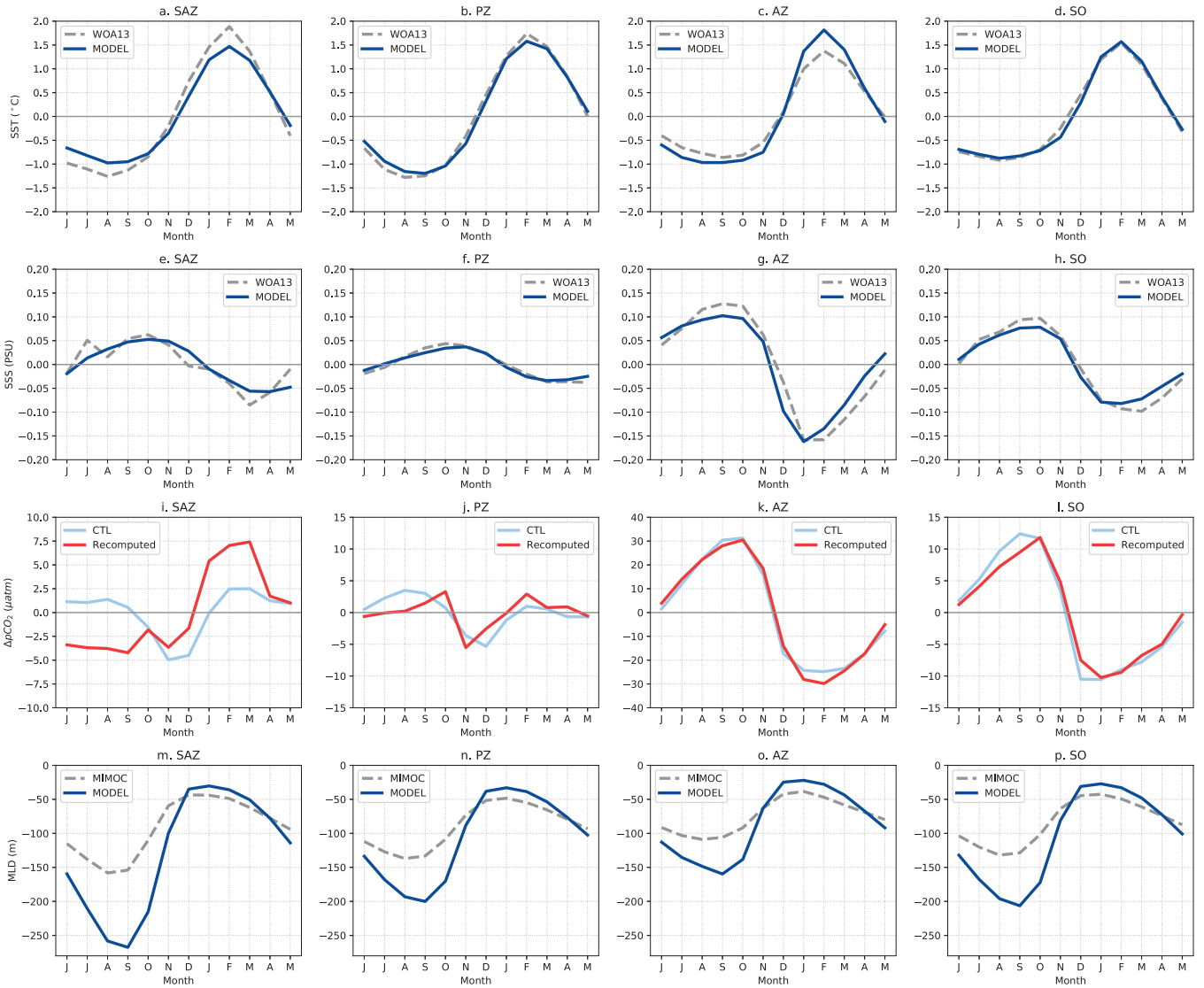

Figure 12. Seasonal cycles from June to May of the average anomalies of (a–d) sea surface temperature (SST) and (e–h) sea surface salinity (SSS) from the World Ocean Atlas 2013 data-based climatologies (dashed lines, gray) and the model (CTL experiment, blue). The second row (i–l) displays the seasonal cycles from June to May of the average anomalies of ΔpCO_2 ($pCO_2^{oc} - pCO_2^{atm}$) from the CTL experiment (light blue) and recomputed with the SST and SSS WOA13 data climatologies and with DIC and alkalinity of the CTL experiment (red). The last row (m–p) displays the seasonal cycles from June to May of the average mixed-layer depth (MLD) from the Monthly Isopycnal and Mixed-layer Ocean Climatology (MIMOC, dashed line, gray) and the model (blue). The columns display from left to right (a, e, i, and m) the Sub-Antarctic Zone (SAZ), (b, f, j, and n) the Polar Zone (PZ), (c, g, k, and o) the Antarctic Zone, and (d, h, l, and p) the Southern Ocean (SO), south of the subtropical front.

Table 7
Statistical Model-Data Comparison of the Two Experiments for Sea Surface Temperature (SST), Sea Surface Salinity (SSS) and Mixed-Layer Depth (MLD) South of 35°S. R, MAE, and AE Are, Respectively, the Correlation Coefficient, the Mean Absolute Error, and the Average Error

	SST (°C)	SSS (psu)	MLD (m)
R	0.98	0.91	0.51
MAE	0.84	0.33	45.6
AE	−0.25	0.31	22.8

The comparison of the seasonal cycles of sea surface temperature (SST) and sea surface salinity (SSS) anomalies between the model and climatological observations shows minor biases in the three hydrological provinces (Figure 12). The model underestimates the seasonal amplitude of SST by 0.7°C in the SAZ (Figure 12a) and by 0.24°C in the PZ (Figure 12b). On the contrary, in the AZ, the model overestimates this amplitude by 0.6°C (Figure 12c). In the whole SO, the amplitude and phase of SST are correctly reproduced (Figure 12d). Regarding SSS anomalies, the seasonal amplitude is very similar between the model and the climatology in each hydrological province (Figures 12e, 12f, and 12g) and globally (Figure 12h). This qualitative comparison is supported by the statistical diagnostics presented in Table 7 where the scores show a good correlation in the spatial patterns of SST and SSS between the model and the observations with R values of 0.98 and 0.91, respectively. The biases between predicted and observed values of SST and SSS expressed in the MAE and the AE exhibit no significant deviations.

In order to quantitatively evaluate the impact of these small biases on pCO_2, we have recomputed the model pCO_2 using the observed values of SST and SSS instead of the simulated values of SST and SSS (Figures 12i, 12j, 12k, and 12l). The results highlight that the solubility effect is well captured by the model as the recomputed seasonal cycle is not significantly altered in the PZ, the AZ and over the SO (Figures 12j, 12k, and 12l). In the SAZ, the recomputed cycle of ΔpCO_2 diverges from the CTL experiment cycle showing that the thermal effect is here underestimated (Figure 12i). This implies that the biological pump should be even stronger than suggested by the model. This gives us further confidence that the representation of the thermodynamic contribution in the model is not responsible for the incorrect seasonality of pCO_2 in the CTL experiment.

Finally, when compared to the Monthly Isopycnal and Mixed-layer Ocean climatology (MIMOC) from Schmidtko et al. (2013), the Mixed-Layer Depth (MLD) in the model is systematically shallower in summer and deeper in winter (Figures 12m, 12n, 12o, and 12p) with a significant discrepancy in the SAZ (Figure 12m). This suggests that the winter entrainment of DIC might be overestimated by the model. In this study, we pointed out that the biases simulated in the CTL experiment result from an insufficient contribution from the biological pump and from winter entrainment (Figures 8a and 8b). Moreover, the model suggests that the intensity of the winter entrainment could be closely linked to the strengthening of the seasonal vertical gradient of DIC induced by the increased biological pump in the PHYSIO experiment (Figure 9). As a consequence, the simulated excessive seasonal amplitude of the MLD cannot be advocated to explain the model discrepancy in the SO. In fact, it should even drive an excessive winter entrainment, which strengthens the hypothesis that the biological pump is largely underestimated in the SO by the CTL experiment.

The above analyses permit us to conclude that the enhanced efficiency of the biological pump in summer does not compensate for an overestimation of the contribution of the solubility effect to the seasonal cycle of pCO_2 in the SO. Furthermore, compared to the solubility effect, the relative contribution of winter entrainment to the seasonal variability of pCO_2 is probably overestimated as a result of an excessive seasonal amplitude of the mixed layer. Both points give us some confidence in the fact that the contribution of the biological pump is underestimated in the CTL experiment and that the adaptive response of diatoms in the SO can be a mechanism by which this biological pump could be strengthened.

4.3. Limitations of the Study

Resolving properly the relative contribution of each process at the scale of the SO and for each hydrological province is challenging because of the high sensitivity of ΔpCO_2. The contrasted results in the SAZ, PZ, and AZ between the observations and the PHYSIO experiment for CHL and ΔpCO_2 reflect the difficulty to represent the contribution of the different environmental factors that shape the plankton community in this oceanic region (Boyd, 2002). They are difficult to diagnose and to disentangle as they are specific for each region (Ardyna et al., 2017). Moreover, the lack of observations at the seasonal scale in the SO makes even more challenging a proper representation of the relative contributions of each component (biological, physical, and thermodynamic) to the seasonal evolution of pCO_2 in this key region for the climate system (Lenton et al., 2006; Majkut et al., 2014; Swart et al., 2015).

The simulated spatial distribution of CHL exhibits quite significant biases. As iron limitation is a major factor controlling primary production in the SO, a point that could be put forward to explain these biases is the complex representation of the different bioavailable sources of iron in the SO (Boyd et al., 2012; Strzepek et al., 2005; Tagliabue et al., 2017). This complexity is not represented in biogeochemical models due to the substantial uncertainties that exist regarding our understanding of the bioavailability of iron to phytoplankton. Another point concerns the size distribution of diatoms which is represented by a single size-class in the model. The composition of diatom communities shows different size-classes in the SO (Froneman et al., 1995; Poulton et al., 2007) with different levels of carbon export efficiency (Froneman, et al., 2004; Lasbleiz et al., 2016; Tréguer et al., 2017). Considering this disparity could have significant implications for the spatial distribution and the seasonal evolution of pCO_2 in the SO.

Finally, the coarse resolution of the model does not allow us to represent with a reliable approximation the dynamical features that drive the availability of nutrients in the sunlit layer. This is illustrated by the biased representation of the variability of MLD in the SO. Preliminary tests with model resolutions of 1 and $^1/_4$ degree did not show any significant improvements in the spatial distribution of both CHL and ΔpCO_2 (not shown). A more realistic behavior could be expected with models at higher resolution (eddy resolving model) that explicitly resolve mesoscale and submesocale dynamical processes (Rosso et al., 2014, 2016).

4.4. Unknown and Uncertainties

Our study suggests that diatoms could grow more efficiently than previously thought in HNLC waters of the SO. This efficiency is inherent to their physiological adaptation strategy to low iron concentrations and to their ability to maintain a relatively high growth rate in spite of a low availability of iron (Strzepek et al., 2011, 2012). This distinctive physiological feature, which is not yet integrated in biogeochemical models, favors diatoms relative to other species and sustains a more significant biological pump with a major impact on the seasonality of surface pCO_2. We modeled this adaptive strategy using a very simple parametrization which alters quite significantly the model behavior, and in our case, improves it. This is a promising first step in our understanding and representation of the role played by the biological component in this region which plays a critical role for the carbon cycle (Arrigo et al., 1998; Marinov et al., 2006).

Our results put forward the decisive role diatoms could have on air-sea CO_2 flux variability but uncertainties remain. The simple formulation adopted in our modeling approach revealed the great sensitivity of surface chlorophyll and pCO_2 to how iron physiology of phytoplankton is represented. It also points out some important unresolved issues. Our proposed parametrization does not rely on a grounded mechanistic understanding of the involved physiological processes. Instead, we imposed a single minimum iron quota for diatoms in iron limited areas south of 45°S. Actually, the SO is characterized by a strong spatial and temporal heterogeneity which is reflected by a high variability in the values of the Fe:C quota (Twining et al., 2004). Such heterogeneity could have an impact on the representation of the spatial patterns of surface chlorophyll but at this stage, not enough is known about this process to better constrain it. Furthermore, our study relies on findings from only two laboratory studies on SO diatom species (Strzepek et al., 2011, 2012). How this adaptive strategy operates and evolves in function of the iron availability, for which species and what is the regional disparity of this strategy are questions that need to be addressed in order to be able to properly resolve this adaptive response at the scale of the SO.

Diatoms are an important group in marine environments and a key phytoplankton group for the carbon cycle (Nelson et al., 1995; Smetacek, 1999). Our modeling study suggests that this group may control to a large extent the seasonal evolution of pCO_2 in the SO. It is thus critical to better understand their physiology and their spatial and temporal distribution in that region. To date, studies on this phytoplankton group have been performed in very localized areas of the SO (Arrigo, 1999; Lasbleiz et al., 2016; Salter et al., 2012; Wright & van den Enden, 2000), which does not provide a synoptic overview of its role. However, other species play an important role in the SO such as *Phaeocystis* (Arrigo, 1999; Coale et al., 2003; DiTullio et al., 2000) or coccolithophores (Balch et al., 2011; Cubillos et al., 2007; Mohan et al., 2008) and may have developed adaptation strategies to support the specific conditions of the SO, although dedicated studies are lacking hitherto. Unfortunately, disentangling the relative contribution from each species and groups to the carbon uptake is still an open question as too few observations are available in the SO to quantify it clearly.

Moreover, the links between the structure of the plankton community and carbon export are largely unknown in the ocean remaining far from being properly modeled (Guidi et al., 2016).

5. Conclusion

This sensitivity study is a first step in highlighting the critical role the physiology of SO diatoms has on the carbon export, the biological pump and the representation of the seasonal cycle of air-sea CO_2 exchange. SO diatoms can efficiently adapt their intracellular Fe requirements to the low availability of iron in order to sustain significant growth rates. Our model finds that this adaptation strategy strengthens the biological pump and significantly modifies the representation of the seasonal variability of CHL and pCO_2 in the SO. This confers a stronger contribution to the biological pump, relative to the effect of solubility and highlights the potentially key role that SO diatom physiology plays for carbon uptake in the upper ocean and export to the ocean interior. However, the modeled solubility effect and winter mixing display biases compared to the observations that affect the robustness of this conclusion. Thus, we highlight the physiological adaptation of SO diatoms to low iron may be a significant biological process that should be considered in our assessments of pCO_2 seasonal dynamics.

Our study demonstrates that some specific biological features may have to be modeled at regional or basin scales for a better integration of the biological component in global models. To improve our understanding of the biological key processes that control both the carbon and iron cycles in the SO, sustained *in situ* observations associated to process-oriented laboratory experiments are needed. It is also essential to explore if this diatom adaptation strategy could occur in other regions like in the iron limited north Pacific or in the north Atlantic where significantly low values of Fe:C quota were measured for several diatom species (Marchetti et al., 2006; Strzepek & Harrison, 2004; Sunda et al., 1991). Such effort is needed to improve the predictive capability of ocean biogeochemical models.

How biological processes and the structure of the phytoplankton ecosystem in the SO will respond to climate change and other stress factors is central to quantify the future evolution of the oceanic carbon sink and higher trophic resources (Bopp et al., 2013; Gattuso et al., 2015). Recent studies suggested that climate change may increase primary production and the abundance of heavily silicified diatoms in the SAZ (Boyd et al., 2015) and in the Ross Sea (Kaufman et al., 2017) designating diatoms as an even possibly stronger key player in the future. This further highlights the need to to urgently improve our understanding of this key phytoplankton group.

Acknowledgments
The model experiments were set up by Christian Ethé. We thank Claire Lo Monaco, Laurent Bopp, Alessandro Tagliabue, and Bruno Delesalle for their help. We would also like to thank Peter Brewer and an anonymous reviewer for their helpful comments that greatly improved this manuscript. The pCO_2 data climatologies were retrieved from the Carbon Data Information Analysis Center (http://cdiac.ornl.gov/ftp/oceans/spco2_1998_2011_ETH_SOM-FFN, http://cdiac.ornl.gov/ftp/oceans/LDEO_Database/Version_2009). The corrected ocean color product was retrieved from Australia's Integrated Marine Observing System (http://imos.org.au/). The sea temperature, sea salinity, and silicate concentration climatologies were downloaded from the National Oceanographic Data Center (https://www.nodc.noaa.gov/OC5/woa13/) and the mixed-layer depth climatology from the Pacific Marine Environmental Laboratory website (https://www.pmel.noaa.gov/mimoc/). The dissolved iron database is available on the GEOTRACES International Data Assemble Centre (https://www.bodc.ac.uk/geotraces/data/historical/). The version of the NEMO code used for this study is freely available at http://www.nemo-ocean.eu. The simulations were performed at IDRIS (France). The model data are available at http://doi.org/10.5281/zenodo.1209155. This study was funded by the EU FP7 project SOCCLI (PIRSES-GA-2012-317699), the ANR project SOBUMS (ANR-16-CE01-0014) and the H2020 project CRESCENDO (grant no. 641816).

References

Alvain, S., Moulin, C., Dandonneau, Y., & Loisel, H. (2008). Seasonal distribution and succession of dominant phytoplankton groups in the global ocean: A satellite view. *Global Biogeochemical Cycles*, *22*, GB3001. https://doi.org/10.1029/2007GB003154

Anav, A., Friedlingstein, P., Kidston, M., Bopp, L., Ciais, P., Cox, P., et al. (2013). Evaluating the land and ocean components of the global carbon cycle in the CMIP5 earth system models. *Journal of Climate*, *26*(18), 6801–6843. https://doi.org/10.1175/JCLI-D-12-00417.1

Ardyna, M., Claustre, H., Sallée, J.-B., D'ovidio, F., Gentili, B., van Dijken, G., et al. (2017). Delineating environmental control of phytoplankton biomass and phenology in the Southern Ocean. *Geophysical Research Letters*, *44*, 5016–5024. https://doi.org/10.1002/2016GL072428

Armbrust, E. V. (2009). The life of diatoms in the world's oceans. *Nature*, *459*(7244), 185–192. https://doi.org/10.1038/nature08057

Arrigo, K. R., Robinson, D. H., Worthen, D. L., Dunbar, D., Tullio, G. R., VanWoert, M., et al. (1999). Phytoplankton community structure and the drawdown of nutrients and CO_2 in the Southern Ocean. *Science*, *283*(5400), 365–367. https://doi.org/10.1126/science.283.5400.365

Arrigo, K. R., & van Dijken, G. L. (2003). Phytoplankton dynamics within 37 Antarctic coastal polynya systems. *Journal of Geophysical Research*, *108*(C8), 3271. https://doi.org/10.1029/2002JC001739

Arrigo, K. R., van Dijken, G. L., & Strong, A. L. (2015). Environmental controls of marine productivity hot spots around Antarctica. *Journal of Geophysical Research: Oceans*, *120*, 5545–5565. https://doi.org/10.1002/2015JC010888

Arrigo, K. R., Worthen, D., Schnell, A., & Lizotte, M. P. (1998). Primary production in Southern Ocean waters. *Journal of Geophysical Research*, *103*(C8), 15587–15600. https://doi.org/10.1029/98JC00930

Assmy, P., Smetacek, V., Montresor, M., Klaas, C., Henjes, J., Strass, V. H., et al. (2013). Thick-shelled, grazer-protected diatoms decouple ocean carbon and silicon cycles in the iron-limited Antarctic Circumpolar Current. *Proceedings of the National Academy of Sciences of the United States of America*, *110*(51), 20633–20638. https://doi.org/10.1073/pnas.1309345110

Aumont, O., Ethé, C., Tagliabue, A., Bopp, L., & Gehlen, M. (2015). PISCES-v2: An ocean biogeochemical model for carbon and ecosystem studies. *Geoscientific Model Development Discussions*, *8*(2), 1375–1509. https://doi.org/10.5194/gmdd-8-1375-2015

Bakker, D. C. E., Pfeil, B., Smith, K., Hankin, S., Olsen, A., Alin, S. R., et al. (2014). An update to the Surface Ocean CO_2 Atlas (SOCAT version 2). *Earth System Science Data*, *6*(1), 69–90. https://doi.org/10.5194/essd-6-69-2014

Balch, W. M., Drapeau, D. T., Bowler, B. C., Lyczskowski, E., Booth, E. S., & Alley, D. (2011). The contribution of coccolithophores to the optical and inorganic carbon budgets during the Southern Ocean Gas Exchange Experiment: New evidence in support of the "Great Calcite Belt" hypothesis. *Journal of Geophysical Research*, *116*, C00F06. https://doi.org/10.1029/2011JC006941

Blain, S., Quéguiner, B., Armand, L., Belviso, S., Bombled, B., Bopp, L., et al. (2007). Effect of natural iron fertilization on carbon sequestration in the Southern Ocean. *Nature*, *446*(7139), 1070–1074. https://doi.org/10.1038/nature05700

Blain, S., Sarthou, G., & Laan, P. (2008). Distribution of dissolved iron during the natural iron-fertilization experiment KEOPS (Kerguelen Plateau, Southern Ocean). *Deep Sea Research, Part II*, *55*(5–7), 594–605. https://doi.org/10.1016/j.dsr2.2007.12.028

Bopp, L., Resplandy, L., Orr, J. C., Doney, S. C., Dunne, J. P., Gehlen, M., et al. (2013). Multiple stressors of ocean ecosystems in the 21st century: Projections with CMIP5 models. *Biogeosciences*, *10*(10), 6225–6245. https://doi.org/10.5194/bg-10-6225-2013

Borrione, I., & Schlitzer, R. (2013). Distribution and recurrence of phytoplankton blooms around South Georgia, Southern Ocean. *Biogeosciences*, *10*(1), 217–231. https://doi.org/10.5194/bg-10-217-2013

Boyd, P. W. (2002). Environmental factors controlling phytoplankton processes in the Southern Ocean. *Journal of Phycology*, *38*(5), 844–861.

Boyd, P. W., Arrigo, K. R., Strzepek, R., & van Dijken, G. L. (2012). Mapping phytoplankton iron utilization: Insights into Southern Ocean supply mechanisms. *Journal of Geophysical Research*, *117*, C06009. https://doi.org/10.1029/2011JC007726

Boyd, P. W., Dillingham, P. W., McGraw, C. M., Armstrong, E. A., Cornwall, C. E., Feng, Y.-Y., et al. (2015). Physiological responses of a Southern Ocean diatom to complex future ocean conditions. *Nature Climate Change*, *6*, 207–213. https://doi.org/10.1038/nclimate2811

Boyd, P. W., Jickells, T., Law, C. S., Blain, S., Boyle, E. A., Buesseler, K. O., et al. (2007). Mesoscale iron enrichment experiments 1993–2005: Synthesis and future directions. *Science*, *315*(5812), 612–617. https://doi.org/10.1126/science.1131669

Brzezinski, M. A. (1985). The Si:C:N ratio of marine diatoms: Interspecific variability and the effect of some environmental variables. *Journal of Phycology*, *21*(3), 347–357.

Bucciarelli, E., Pondaven, P., & Sarthou, G. (2010). Effects of an iron-light co-limitation on the elemental composition (Si, C, N) of the marine diatoms *Thalassiosira oceanica* and *Ditylum brightwellii*. *Biogeosciences*, *7*(2), 657–669.

Buesseler, K. O., Ball, L., Andrews, J., Cochran, J. K., Hirschberg, D. J., Bacon, M. P., et al. (2001). Upper ocean export of particulate organic carbon and biogenic silica in the Southern Ocean along 170 W. *Deep Sea Research, Part II*, *48*(19), 4275–4297.

Buitenhuis, E. T., & Geider, R. J. (2010). A model of phytoplankton acclimation to iron-light colimitation. *Limnology and Oceanography Methods*, *55*(2), 714–724.

Cavan, E. L., Le Moigne, F. A. C., Poulton, A. J., Tarling, G. A., Ward, P., Daniels, C. J., et al. (2015). Attenuation of particulate organic carbon flux in the Scotia Sea, Southern Ocean, is controlled by zooplankton fecal pellets: Scotia sea carbon fluxes. *Geophysical Research Letters*, *42*, 821–830. https://doi.org/10.1002/2014GL062744

Coale, K. H., Wang, X., Tanner, S. J., & Johnson, K. S. (2003). Phytoplankton growth and biological response to iron and zinc addition in the Ross Sea and Antarctic Circumpolar Current along 170 W. *Deep Sea Research, Part II*, *50*(3), 635–653.

Comiso, J. C., McClain, C. R., Sullivan, C. W., Ryan, J. P., & Leonard, C. L. (1993). Coastal Zone Color Scanner pigment concentrations in the Southern Ocean and relationships to geophysical surface features. *Journal of Geophysical Research*, *98*(C2), 2419–2451.

Cubillos, J., Wright, S., Nash, G., de Salas, M., Griffiths, B., Tilbrook, B., et al. (2007). Calcification morphotypes of the coccolithophorid *Emiliania huxleyi* in the Southern Ocean: Changes in 2001 to 2006 compared to historical data. *Marine Ecology Progress Series*, *348*, 47–54. https://doi.org/10.3354/meps07058

de Baar, H. J. W. (2005). Synthesis of iron fertilization experiments: From the iron age in the age of enlightenment. *Journal of Geophysical Research*, *110*, C09S16.https://doi.org/10.1029/2004JC002601

DiTullio, G. R., Grebmeier, J. M., Arrigo, K. R., Lizotte, M. P., Robinson, D. H., Leventer, A., et al. (2000). Rapid and early export of *Phaeocystis antarctica* blooms in the Ross Sea, Antarctica. *Nature*, *404*(6778), 595–598.

Drum, R. W., & Gordon, R. (2003). Star Trek replicators and diatom nanotechnology. *Trends in Biotechnology*, *21*(8), 325–328.

Ducklow, H. W., Erickson, M., Kelly, J., Montes-Hugo, M., Ribic, C. A., Smith, R. C., et al. (2008). Particle export from the upper ocean over the continental shelf of the west Antarctic Peninsula: A long-term record, 1992–2007. *Deep Sea Research, Part II*, *55*(18–19), 2118–2131. https://doi.org/10.1016/j.dsr2.2008.04.028

Falkowski, P. G., Barber, R. T., & Smetacek, V. (1998). Biogeochemical controls and feedbacks on ocean primary production. *Science*, *281*(5374), 200–206.

Flynn, K. J., & Hipkin, C. R. (1999). Interactions between iron, light, ammonium, and nitrate: Insights from the construction of a dynamic model of algal physiology. *Journal of Phycology*, *35*(6), 1171–1190.

Froneman, P. W., McQuaid, C. D., & Perissinotto, R. (1995). Biogeographic structure of the microphytoplankton assemblages of the south Atlantic and Southern Ocean during austral summer. *Journal of Plankton Research*, *17*(9), 1791–1802.

Froneman, P. W., Pakhomov, E. A., & Balarin, M. G. (2004). Size-fractionated phytoplankton biomass, production and biogenic carbon flux in the eastern Atlantic sector of the Southern Ocean in late austral summer 1997–1998. *Deep Sea Research, Part II*, *51*(22–24), 2715–2729. https://doi.org/10.1016/j.dsr2.2002.09.001

Gaspar, P., Gregoris, Y., & Lefevre, J.-M. (1990). A simple eddy kinetic energy model for simulations of the oceanic vertical mixing: Tests at station Papa and Long-Term Upper Ocean Study site. *Journal of Geophysical Research*, *95*(C9), 16179–16193.

Gattuso, J.-P., Magnan, A., Bille, R., Cheung, W. W. L., Howes, E. L., Joos, F., et al. (2015). Contrasting futures for ocean and society from different anthropogenic CO_2 emissions scenarios. *Science*, *349*(6243), aac4722. https://doi.org/10.1126/science.aac4722

Gent, P. R., & McWilliams, J. C. (1990). Isopycnal mixing in ocean circulation models. *Journal of Physical Oceanography*, *20*(1), 150–155.

Gruber, N., Gloor, M., Mikaloff Fletcher, S. E., Doney, S. C., Dutkiewicz, S., Follows, M. J., et al. (2009). Oceanic sources, sinks, and transport of atmospheric CO_2. *Global Biogeochemical Cycles*, *23*, GB1005. https://doi.org/10.1029/2008GB003349

Guidi, L., Chaffron, S., Bittner, L., Eveillard, D., Larhlimi, A., Roux, S., et al. (2016). Plankton networks driving carbon export in the oligotrophic ocean. *Nature*, *532*(7600), 465–470. https://doi.org/10.1038/nature16942

Hoffmann, L. J., Peeken, I., & Lochte, K. (2007). Effects of iron on the elemental stoichiometry during EIFEX and in the diatoms *Fragilariopsis kerguelensis* and *Chaetoceros dichaeta*. *Biogeosciences*, *4*(4), 569–579.

Johnson, R., Strutton, P. G., Wright, S. W., McMinn, A., & Meiners, K. M. (2013). Three improved satellite chlorophyll algorithms for the Southern Ocean. *Journal of Geophysical Research: Oceans*, *118*, 3694–3703. https://doi.org/10.1002/jgrc.20270

Kaufman, D. E., Friedrichs, M. A. M., Smith, W. O., Hofmann, E. E., Dinniman, M. S., & Hemmings, J. C. P. (2017). Climate change impacts on southern Ross Sea phytoplankton composition, productivity, and export. *Journal of Geophysical Research: Oceans*, *122*, 2339–2359. https://doi.org/10.1002/2016JC012514

Khatiwala, S., Tanhua, T., Mikaloff Fletcher, S., Gerber, M., Doney, S. C., Graven, H. D., et al. (2013). Global ocean storage of anthropogenic carbon. *Biogeosciences*, *10*(4), 2169–2191. https://doi.org/10.5194/bg-10-2169-2013

Korb, R., Whitehouse, M., Atkinson, A., & Thorpe, S. (2008). Magnitude and maintenance of the phytoplankton bloom at South Georgia: A naturally iron-replete environment. *Marine Ecology Progress Series*, *368*, 75–91. https://doi.org/10.3354/meps07525

Kustka, A. B., Allen, A. E., & Morel, F. M. M. (2007). Sequence analysis and transcriptional regulation of iron acquisition genes in two marine diatoms. *Journal of Phycology*, *43*(4), 715–729. https://doi.org/10.1111/j.1529-8817.2007.00359.x

Lam, P. J., & Bishop, J. K. B. (2007). High biomass, low export regimes in the Southern Ocean. *Deep Sea Research, Part II*, *54*(5–7), 601–638. https://doi.org/10.1016/j.dsr2.2007.01.013

Landschützer, P., Gruber, N., Bakker, D. C. E., & Schuster, U. (2014). Recent variability of the global ocean carbon sink. *Global Biogeochemical Cycles*, *28*(9), 927–949. https://doi.org/10.1002/2014GB004853

Lasbleiz, M., Leblanc, K., Armand, L. K., Christaki, U., Georges, C., Obernosterer, I., et al. (2016). Composition of diatom communities and their contribution to plankton biomass in the naturally iron-fertilized region of Kerguelen in the Southern Ocean. *FEMS Microbiology Ecology*, *92*(11), fiw171.

Lasbleiz, M., Leblanc, K., Blain, S., Ras, J., Cornet-Barthaux, V., Hélias Nunige, S., et al. (2014). Pigments, elemental composition (C, N, P, and Si), and stoichiometry of particulate matter in the naturally iron fertilized region of Kerguelen in the Southern Ocean. *Biogeosciences*, *11*(20), 5931–5955. https://doi.org/10.5194/bg-11-5931-2014

Laurenceau-Cornec, E. C., Trull, T. W., Davies, D. M., Bray, S. G., Doran, J., Planchon, F., et al. (2015). The relative importance of phytoplankton aggregates and zooplankton fecal pellets to carbon export: Insights from free-drifting sediment trap deployments in naturally iron-fertilised waters near the Kerguelen Plateau. *Biogeosciences*, *12*(4), 1007–1027. https://doi.org/10.5194/bg-12-1007-2015

Le Moigne, F. A. C., Henson, S. A., Cavan, E., Georges, C., Pabortsava, K., Achterberg, E. P., et al. (2016). What causes the inverse relationship between primary production and export efficiency in the Southern Ocean?. *Geophysical Research Letters*, *43*, 4457–4466. https://doi.org/10.1002/2016GL068480

Leggett, R. W., & Williams, L. R. (1981). A reliability index for models. *Ecological Modelling*, *13*(4), 303–312.

Lengaigne, M., Madec, G., Menkes, C., & Alory, G. (2003). Impact of isopycnal mixing on the tropical ocean circulation. *Journal of Geophysical Research*, *108*(C11), 3345. https://doi.org/10.1029/2002JC001704

Lenton, A., Matear, R. J., & Tilbrook, B. (2006). Design of an observational strategy for quantifying the Southern Ocean uptake of CO_2. *Global Biogeochemical Cycles*, *20*, GB4010. https://doi.org/10.1029/2005GB002620

Lenton, A., Metzl, N., Takahashi, T., Kuchinke, M., Matear, R. J., Roy, T., et al. (2012). The observed evolution of oceanic pCO_2 and its drivers over the last two decades. *Global Biogeochemical Cycles*, *26*, GB2021. https://doi.org/10.1029/2011GB004095

Lenton, A., Tilbrook, B., Law, R. M., Bakker, D., Doney, S. C., Gruber, N., et al. (2013). Sea-air CO_2 fluxes in the Southern Ocean for the period 1990–2009. *Biogeosciences*, *10*(6), 4037–4054. https://doi.org/10.5194/bg-10-4037-2013

Lévy, M., Iovino, D., Resplandy, L., Klein, P., Madec, G., Tréguier, A.-M., et al. (2012). Large-scale impacts of submesoscale dynamics on phytoplankton: Local and remote effects. *Ocean Modelling*, *43–44*, 77–93. https://doi.org/10.1016/j.ocemod.2011.12.003

Madec, G. (2008). *NEMO ocean engine* (Vol. 27, pp. 1–217). Paris, France: Note Du Pole de Modélisation de l'Institut Pierre-Simon Laplace.

Maiti, K., Charette, M. A., Buesseler, K. O., & Kahru, M. (2013). An inverse relationship between production and export efficiency in the Southern Ocean. *Geophysical Research Letters*, *40*, 1557–1561. https://doi.org/10.1002/grl.50219

Majkut, J. D., Carter, B. R., Frolicher, T. L., Dufour, C. O., Rodgers, K. B., & Sarmiento, J. L. (2014). An observing system simulation for Southern Ocean carbon dioxide uptake. *Philosophical Transactions of the Royal Society A*, *372*(2019), 20130046. https://doi.org/10.1098/rsta.2013.0046

Marchetti, A., Maldonado, M. T., Lane, E. S., & Harrison, P. J. (2006). Iron requirements of the pennate diatom Pseudonitzschia: Comparison of oceanic (high-nitrate, low-chlorophyll waters) and coastal species. *Limnology and Oceanography Methods*, *51*(5), 2092–2101.

Marinov, I., Gnanadesikan, A., Toggweiler, J. R., & Sarmiento, J. L. (2006). The Southern Ocean biogeochemical divide. *Nature*, *441*(7096), 964–967. https://doi.org/10.1038/nature04883

Martin, J., H., Fitzwater, S., E., & Gordon, M., R. (1990). Iron deficiency limits phytoplankton in Antarctic waters. *Global Biogeochemical Cycles*, *4*(1), 5–12.

Martin-Jézéquel, V., Hildebrand, M., & Brzezinski, M. A. (2000). Silicon metabolism in diatoms: Implications for growth. *Journal of Phycology*, *36*(5), 821–840.

Mashayek, A., Ferrari, R., Merrifield, S., Ledwell, J. R., St Laurent, L., & Garabato, A. N. (2017). Topographic enhancement of vertical turbulent mixing in the Southern Ocean. *Nature Communications*, *8*, 14197. https://doi.org/10.1038/ncomms14197

Merlivat, L., Boutin, J., & Antoine, D. (2015). Roles of biological and physical processes in driving seasonal air-sea CO_2 flux in the Southern Ocean: New insights from CARIOCA pCO_2. *Journal of Marine Systems*, *147*, 9–20. https://doi.org/10.1016/j.jmarsys.2014.04.015

Metzl, N. (2009). Decadal increase of oceanic carbon dioxide in Southern Indian Ocean surface waters (1991–2007). *Deep Sea Research, Part II*, *56*(8–10), 607–619. https://doi.org/10.1016/j.dsr2.2008.12.007

Metzl, N., Brunet, C., Jabaud-Jan, A., Poisson, A., & Schauer, B. (2006). Summer and winter air–sea CO2 fluxes in the Southern Ocean. *Deep Sea Research, Part I*, *53*(9), 1548–1563. https://doi.org/10.1016/j.dsr.2006.07.006

Mohan, R., Mergulhao, L. P., Guptha, M. V. S., Rajakumar, A., Thamban, M., AnilKumar, N., et al. (2008). Ecology of coccolithophores in the Indian sector of the Southern Ocean. *Marine Micropaleontology*, *67*(1–2), 30–45. https://doi.org/10.1016/j.marmicro.2007.08.005

Mongwe, N. P., Chang, N., & Monteiro, P. M. S. (2016). The seasonal cycle as a mode to diagnose biases in modelled CO_2 fluxes in the Southern Ocean. *Ocean Modelling*, *106*, 90–103. https://doi.org/10.1016/j.ocemod.2016.09.006

Monteiro, P. M. S., Gregor, L., Lévy, M., Maenner, S., Sabine, C. L., & Swart, S. (2015). Intraseasonal variability linked to sampling alias in air-sea CO_2 fluxes in the Southern Ocean. *Geophysical Research Letters*, *42*, 8507–8514. https://doi.org/10.1002/2015GL066009

Moore, J. K., & Abbott, M. R. (2000). Phytoplankton chlorophyll distributions and primary production in the Southern Ocean. *Journal of Geophysical Research*, *105*(C12), 28709–28722. https://doi.org/10.1029/1999JC000043

Morris, P. J., Sanders, R., Turnewitsch, R., & Thomalla, S. (2007). 234Th-derived particulate organic carbon export from an island-induced phytoplankton bloom in the Southern Ocean. *Deep Sea Research, Part II*, *54*(18–20), 2208–2232. https://doi.org/10.1016/j.dsr2.2007.06.002

Nash, J. E., & Sutcliffe, J. V. (1970). River flow forecasting through conceptual models. Part I—A discussion of principles. *Journal of Hydrology*, *10*(3), 282–290.

Nelson, D. M., Tréguier, P., Brzenski, M. A., Leynaert, A., & Quéguiner, B. (1995). Production and dissolution of biogenic silica in the ocean: Revised global estimates, comparison with regional data and relationship to biogenic sedimentation. *Global Biogeochemical Cycles*, *9*(3), 359–372.

Orsi, A., H., Whitworth, T. III, & Nowlin, W. D. Jr. (1995). On the meridional extent and fronts of the Antarctic circumpolar current. *Deep Sea Research, Part I*, *42*(5), 641–673.

Pollard, R. T., Salter, I., Sanders, R. J., Lucas, M. I., Moore, C. M., Mills, R. A., et al. (2009). Southern Ocean deep-water carbon export enhanced by natural iron fertilization. *Nature*, *457*(7229), 577–580. https://doi.org/10.1038/nature07716

Pollard, R. T., Sanders, R., Lucas, M., & Statham, P. (2007). The Crozet natural iron bloom and export experiment (CROZEX). *Deep Sea Research, Part II*, *54*(18–20), 1905–1914. https://doi.org/10.1016/j.dsr2.2007.07.023

Pondaven, P., Ragueneau, O., Treguer, P., Hauvespre, A., Dezileau, L., & Reyss, J.-L. (2000). Resolving the 'opal paradox' in the Southern Ocean. *Nature*, *405*(6783), 168–172.

Poulton, A. J., Mark Moore, C., Seeyave, S., Lucas, M. I., Fielding, S., & Ward, P. (2007). Phytoplankton community composition around the Crozet Plateau, with emphasis on diatoms and *Phaeocystis*. *Deep Sea Research, Part II*, *54*(18–20), 2085–2105. https://doi.org/10.1016/j.dsr2.2007.06.005

Puigcorbé, V., Roca-Martí, M., Masqué, P., Benitez-Nelson, C. R., Rutgers v. d. Loeff, M., Laglera, L. M., et al. (2017). Particulate organic carbon export across the Antarctic Circumpolar Current at 10°E: Differences between north and south of the Antarctic Polar Front. *Deep Sea Research, Part II*, *138*, 86–101. https://doi.org/10.1016/j.dsr2.2016.05.016

Quéguiner, B., & Brzezinski, M. A. (2002). Biogenic silica production rates and particulate organic matter distribution in the Atlantic sector of the Southern Ocean during austral spring 1992. *Deep Sea Research, Part II*, *49*(9), 1765–1786.

Rembauville, M., Blain, S., Armand, L., Quéguiner, B., & Salter, I. (2015). Export fluxes in a naturally iron-fertilized area of the Southern Ocean—Part 2: Importance of diatom resting spores and faecal pellets for export. *Biogeosciences*, *12*(11), 3171–3195. https://doi.org/10.5194/bg-12-3171-2015

Rembauville, M., Manno, C., Tarling, G. A., Blain, S., & Salter, I. (2016). Strong contribution of diatom resting spores to deep-sea carbon transfer in naturally iron-fertilized waters downstream of South Georgia. *Deep Sea Research, Part I*, *115*, 22–35. https://doi.org/10.1016/j.dsr.2016.05.002

Resplandy, L., Boutin, J., & Merlivat, L. (2014). Observed small spatial scale and seasonal variability of the CO_2 system in the Southern Ocean. *Biogeosciences*, *11*(1), 75–90. https://doi.org/10.5194/bg-11-75-2014

Rigual-Hernández, A. S., Trull, T. W., Bray, S. G., & Armand, L. K. (2016). The fate of diatom valves in the Subantarctic and Polar Frontal Zones of the Southern Ocean: Sediment trap versus surface sediment assemblages. *Palaeogeography, Palaeoclimatology, Palaeoecology*, *457*, 129–143. https://doi.org/10.1016/j.palaeo.2016.06.004

Rigual-Hernández, A. S., Trull, T. W., Bray, S. G., Closset, I., & Armand, L. K. (2015a). Seasonal dynamics in diatom and particulate export fluxes to the deep sea in the Australian sector of the southern Antarctic Zone. *Journal of Marine Systems*, *142*, 62–74. https://doi.org/10.1016/j.jmarsys.2014.10.002

Rigual-Hernández, A. S., Trull, T. W., Bray, S. G., Cortina, A., & Armand, L. K. (2015b). Latitudinal and temporal distributions of diatom populations in the pelagic waters of the Subantarctic and Polar Frontal zones of the Southern Ocean and their role in the biological pump. *Biogeosciences*, *12*(18), 5309–5337. https://doi.org/10.5194/bg-12-5309-2015

Roca-Martí, M., Puigcorbé, V., Iversen, M. H., van der Loeff, M. R., Klaas, C., Cheah, W., et al. (2017). High particulate organic carbon export during the decline of a vast diatom bloom in the Atlantic sector of the Southern Ocean. *Deep Sea Research, Part II*, *138*, 102–115. https://doi.org/10.1016/j.dsr2.2015.12.007

Rosso, I., Hogg, A. M., Kiss, A. E., & Gayen, B. (2015). Topographic influence on submesoscale dynamics in the Southern Ocean. *Geophysical Research Letters*, *42*, 1139–1147. https://doi.org/10.1002/2014GL062720

Rosso, I., Hogg, A. M., Matear, R., & Strutton, P. G. (2016). Quantifying the influence of sub-mesoscale dynamics on the supply of iron to Southern Ocean phytoplankton blooms. *Deep Sea Research, Part I*, *115*, 199–209. https://doi.org/10.1016/j.dsr.2016.06.009

Rosso, I., Hogg, A. M., Strutton, P. G., Kiss, A. E., Matear, R., Klocker, A., et al. (2014). Vertical transport in the ocean due to sub-mesoscale structures: Impacts in the Kerguelen region. *Ocean Modelling*, *80*, 10–23. https://doi.org/10.1016/j.ocemod.2014.05.001

Round, F. E., Crawford, R. M., & Mann, D. G. (1990). *Diatoms: Biology and morphology of the genera*. Cambridge, UK: Cambridge University Press.

Rousseaux, C., & Gregg, W. (2013). Interannual variation in phytoplankton primary production at a global scale. *Remote Sensing*, *6*(1), 1–19. https://doi.org/10.3390/rs6010001

Sabine, C. L., Feely, R. A., Gruber, N., Key, R. M., Lee, K., Bullister, J. L. . . . Others, (2004). The oceanic sink for anthropogenic CO_2. *Science*, *305*(5682), 367–371.

Salter, I., Kemp, A. E. S., Moore, C. M., Lampitt, R. S., Wolff, G. A., & Holtvoeth, J. (2012). Diatom resting spore ecology drives enhanced carbon export from a naturally iron-fertilized bloom in the Southern Ocean. *Global Biogeochemical Cycles*, *26*, GB1014. https://doi.org/10.1029/2010GB003977

Sarthou, G., Timmermans, K. R., Blain, S., & Tréguer, P. (2005). Growth physiology and fate of diatoms in the ocean: A review. *Journal of Sea Research*, *53*(1–2), 25–42. https://doi.org/10.1016/j.seares.2004.01.007

Schmidtko, S., Johnson, G. C., & Lyman, J. M. (2013). MIMOC: A global monthly isopycnal upper-ocean climatology with mixed layers. *Journal of Geophysical Research: Oceans*, *118*, 1658–1672. https://doi.org/10.1002/jgrc.20122

Shadwick, E. H., Trull, T. W., Tilbrook, B., Sutton, A. J., Schulz, E., & Sabine, C. L. (2015). Seasonality of biological and physical controls on surface ocean CO from hourly observations at the Southern Ocean Time Series site south of Australia. *Global Biogeochemical Cycles*, *29*, 223–238. https://doi.org/10.1002/2014GB004906

Smetacek, V. (1999). Diatoms and the ocean carbon cycle. *Protist*, *150*(1), 25–32.

Smith, R. C., Martinson, D. G., Stammerjohn, S. E., Iannuzzi, R. A., & Ireson, K. (2008). Bellingshausen and western Antarctic Peninsula region: Pigment biomass and sea-ice spatial/temporal distributions and interannual variabilty. *Deep Sea Research, Part II*, *55*(18–19), 1949–1963. https://doi.org/10.1016/j.dsr2.2008.04.027

Stow, C. A., Jolliff, J., McGillicuddy, D. J., Doney, S. C., Allen, J. I., Friedrichs, M. A. M., et al. (2009). Skill assessment for coupled biological/physical models of marine systems. *Journal of Marine Systems*, *76*(1–2), 4–15. https://doi.org/10.1016/j.jmarsys.2008.03.011

Strzepek, R. F., & Harrison, P. J. (2004). Photosynthetic architecture differs in coastal and oceanic diatoms. *Nature*, *431*(7009), 689–692. https://doi.org/10.1038/nature02890

Strzepek, R. F., Hunter, K. A., Frew, R. D., Harrison, P. J., & Boyd, P. W. (2012). Iron-light interactions differ in Southern Ocean phytoplankton. *Limnology and Oceanography Methods*, *57*(4), 1182–1200. https://doi.org/10.4319/lo.2012.57.4.1182

Strzepek, R. F., Maldonado, M. T., Higgins, J. L., Hall, J., Safi, K., Wilhelm, S. W., et al. (2005). Spinning the ''Ferrous Wheel'': The importance of the microbial community in an iron budget during the FeCycle experiment. *Global Biogeochemical Cycles*, *19*, GB4S26. https://doi.org/10.1029/2005GB002490

Strzepek, R. F., Maldonado, M. T., Hunter, K. A., Frew, R. D., & Boyd, P. W. (2011). Adaptive strategies by Southern Ocean phytoplankton to lessen iron limitation: Uptake of organically complexed iron and reduced cellular iron requirements. *Limnology and Oceanography Methods*, *56*(6), 1983–2002. https://doi.org/10.4319/lo.2011.56.6.1983

Sullivan, C. W., Arrigo, K. R., McClain, C. R., Comiso, J. C., & Firestone, J. (1993). Distributions of phytoplankton blooms in the Southern Ocean. *Science-AAAS-Weekly Paper Edition-Including Guide to Scientific Information*, *262*(5141), 1832–1837.

Sunda, W. G., Swift, D. G., & Huntsman, S. A. (1991). Low iron requirement for growth in oceanic phytoplankton. *Nature*, *351*, 55–57.

Swart, S., Thomalla, S. J., & Monteiro, P. M. S. (2015). The seasonal cycle of mixed layer dynamics and phytoplankton biomass in the Sub-Antarctic Zone: A high-resolution glider experiment. *Journal of Marine Systems*, *147*, 103–115. https://doi.org/10.1016/j.jmarsys.2014.06.002

Tagliabue, A., Bowie, A. R., Boyd, P. W., Buck, K. N., Johnson, K. S., & Saito, M. A. (2017). The integral role of iron in ocean biogeochemistry. *Nature*, *543*(7643), 51–59. https://doi.org/10.1038/nature21058

Tagliabue, A., Mtshali, T., Aumont, O., Bowie, A. R., Klunder, M. B., Roychoudhury, A. N., et al. (2012). A global compilation of dissolved iron measurements: Focus on distributions and processes in the Southern Ocean. *Biogeosciences*, *9*(6), 2333–2349. https://doi.org/10.5194/bg-9-2333-2012

Takahashi, T., Olafsson, J., & Goddard, J. G. (1993). Seasonal variation of CO_2 and nutrients. *Global Biogeochemical Cycles*, *7*(4), 843–878.

Takahashi, T., Sutherland, S. C., Wanninkhof, R., Sweeney, C., Feely, R. A., Chipman, D. W., et al. (2009). Climatological mean and decadal change in surface ocean pCO2, and net sea-air CO_2 flux over the global oceans. *Deep Sea Research, Part II*, *56*(8–10), 554–577. https://doi.org/10.1016/j.dsr2.2008.12.009

Takahashi, T., Sweeney, C., Hales, B., Chipman, D., Newberger, T., Goddard, J., et al. (2012). The changing carbon cycle in the Southern Ocean. *Oceanography*, *25*(3), 26–37. https://doi.org/10.5670/oceanog.2012.71

Thomalla, S. J., Fauchereau, N., Swart, S., & Monteiro, P. M. S. (2011). Regional scale characteristics of the seasonal cycle of chlorophyll in the Southern Ocean. *Biogeosciences*, *8*(10), 2849–2866. https://doi.org/10.5194/bg-8-2849-2011

Timmermann, R., Goosse, H., Madec, G., Fichefet, T., Ethe, C., & Dulière, V. (2005). On the representation of high latitude processes in the ORCA-LIM global coupled sea ice-ocean model. *Ocean Modelling*, *8*(1–2), 175–201. https://doi.org/10.1016/j.ocemod.2003.12.009

Tréguer, P. J., Bowler, C., Moriceau, B., Dutkiewicz, S., Gehlen, M., Aumont, O., et al. (2017). Influence of diatom diversity on the ocean biological carbon pump. *Nature Geoscience*, *11*, 27–37. https://doi.org/10.1038/s41561-017-0028-x

Tréguer, P. J., & De La Rocha, C. L. (2013). The World Ocean silica cycle. *Annual Review of Marine Science*, *5*(1), 477–501. https://doi.org/10.1146/annurev-marine-121211-172346

Tréguer, P. J., & Pondaven, P. (2000). Silica control of carbon dioxyde. *Nature*, *406*(6794), 358–359.

Twining, B. S., Baines, S. B., Fisher, N. S., & Landry, M. R. (2004). Cellular iron contents of plankton during the Southern Ocean Iron Experiment (SOFeX). *Deep Sea Research, Part I*, *51*(12), 1827–1850. https://doi.org/10.1016/j.dsr.2004.08.007

Tyrrell, T., Merico, A., Waniek, J. J., Wong, C. S., Metzl, N., & Whitney, F. (2005). Effect of seafloor depth on phytoplankton blooms in high-nitrate, low-chlorophyll (HNLC) regions. *Journal of Geophysical Research*, *110*, G02007. https://doi.org/10.1029/2005JG000041

Wanninkhof, R. (1992). Relationship between wind speed and gas exchange over the ocean. *Journal of Geophysical Research*, *97*(C5), 7373–7382.

Williams, N. L., Juranek, L. W., Feely, R. A., Johnson, K. S., Sarmiento, J. L., Talley, L. D., et al. (2017). Calculating surface ocean pCO_2 from biogeochemical Argo floats equipped with pH: An uncertainty analysis. *Global Biogeochemical Cycles*, *31*, 591–604. https://doi.org/10.1002/2016GB005541

Wright, S. W., & van den Enden, R. L. (2000). Phytoplankton community structure and stocks in the East Antarctic marginal ice zone (BROKE survey, January–March 1996) determined by CHEMTAX analysis of HPLC pigment signatures. *Deep Sea Research, Part II*, *47*(12), 2363–2400.